



HAL
open science

A Simple Finite-Volume Method for Compressible Isothermal Two-Phase Flows Simulation

F Caro, F Coquel, Damien Jamet, S Kokh

► **To cite this version:**

F Caro, F Coquel, Damien Jamet, S Kokh. A Simple Finite-Volume Method for Compressible Isothermal Two-Phase Flows Simulation. International Journal on Finite Volumes, 2006, www.latp.univ-mrs.fr/IJFV. hal-01114190

HAL Id: hal-01114190

<https://hal.science/hal-01114190>

Submitted on 9 Feb 2015

HAL is a multi-disciplinary open access archive for the deposit and dissemination of scientific research documents, whether they are published or not. The documents may come from teaching and research institutions in France or abroad, or from public or private research centers.

L'archive ouverte pluridisciplinaire **HAL**, est destinée au dépôt et à la diffusion de documents scientifiques de niveau recherche, publiés ou non, émanant des établissements d'enseignement et de recherche français ou étrangers, des laboratoires publics ou privés.

A Simple Finite-Volume Method for Compressible Isothermal Two-Phase Flows Simulation

F. Caro^a

^a *ONERA Châtillon, BP 72, 92322 Châtillon Cedex, France*

florian.caro@onera.fr

F. Coquel^b

^b *LJLL, Paris VI University, 75013 Paris, France*

coquel@ann.jussieu.fr

D. Jamet^c

^c *CEA Grenoble, 17 rue des Martyrs, 38054 Grenoble Cedex 9, France*

didier.jamet@cea.fr

S. Kokh^d

^d *CEA Saclay, 91191 Gif-sur-Yvette Cedex, France*

samuel.kokh@cea.fr

Abstract

We present a simple method for simulating isothermal compressible two-phase flows with mass transfer. The convective part of the model is compatible with the Least Action Principle and the system is endowed with an entropy inequality which accounts for phase change terms and phasic pressure unbalance. A study of the system as a relaxed model of two equilibrium models is performed. This study allows the design of two-step relaxation-convection Finite-Volume discretization scheme which complies with the entropy balance of the model which drives the mass transfer phase-change process. Numerical results involving dynamical phase-change are presented.

Key words : hyperbolic systems, relaxation, phase-change.

1 Introduction

In the past years encouraging contributions have been proposed by several authors [1, 2, 9, 19, 15] for the description of mesoscale interface compressible two-phase flows using different numbers of independent variables. These models have in common a single-velocity kinematics and most of them do not account for phase change phenomena. Nevertheless more recent contributions tend to show that two-phase flows with mass transfer can also be modelled with a single velocity system [15, 16, 3, 14]. Let us also mention the work of Le Métayer [20] which models mass transfer within the framework of an average model by the mean of a kinetic relation.

In the present paper we will present a system which is based on a relaxation approach which naturally accounts for mass transfer in a thermodynamically consistent way along with a natural Finite-Volume discretization method that complies with the thermodynamical features of the system.

For the sake of simplicity, we suppose that the flow is isothermal. While this assumption does not allow an all-purpose realistic energy exchange, it is not unreasonable since for small scales interface flow, phase change can occur at thermal equilibrium (see *e.g.* [10]). An important feature of the proposed model is that it is compatible with a description of the local mechanical and thermodynamical equilibria of the interface without any parameter prescribing the evaporation rate.

This work departs from the classical van der Waals type phase change modelling which usually requires additional terms related to very small scale effects (see [15]). These are intended to correct the core system intrinsic lack of hyperbolicity. A drawback of this approach is that it requires numerical strategies to use very fine discretizing grids. On the contrary, the present system is fully compliant with standard numerical relaxation techniques for hyperbolic systems although the model equilibrium states are compatible with the equilibrium Maxwell points for a van der Waals law.

The paper is structured as follows: we first derive a primitive system using classical mechanics arguments: we first use a Least Action Principle to derive the conservative part of the system. Then we add dissipative structures to the system by designing an entropy inequality. This entropy evolution equation will provide the system with source terms that account for the fact that mass transfer and pressure are unbalanced between phases. Two different systems will then be derived by considering the equilibria which correspond to instantaneous relaxations due to the source terms. After a study of these systems, we will present the two-step convection-relaxation numerical strategy we use to approximate the equilibrium systems solution. Finally we present numerical tests involving the simulation of dynamical phase-change phenomena.

2 System Modelling

The modelling task we achieve here is based on standard mechanics arguments which have been used by several authors in various contexts from the classical Euler equations to fluids of second grade. For instance we refer the reader to [8, 11, 22, 23] and the references therein. It boils down to a “roadmap” which consists in first defining

the set of variables that will be used to describe the state of the system, postulating a Lagrangian energy associated with the system. The Least Action Principle provides the conservative part of the system, a system entropy inequality provides the dissipative terms.

2.1 General Modelling Assumptions

The starting point of our programme deals with defining the system variables. Let ρ_α be the density of the phase $\alpha = 1, 2$ and z be an abstract order parameter which characterizes the phase 1. Noting $z_1 = z$ and $z_2 = 1 - z$, we define the system density ρ by

$$\rho = z\rho_1 + (1 - z)\rho_2.$$

We denote respectively by $y = y_1 = \rho_1 z_1 / \rho$ and $y_2 = 1 - y = \rho_2 z_2 / \rho$ the phase $\alpha = 1, 2$ mass fraction. Phases are supposed to share the same velocity \mathbf{u} and we note $\mathbf{j} = \rho\mathbf{u}$ the fluid global momentum. We first suppose that the system free energy f depends solely on the variables (ρ, y, z) , namely $f = f(\rho, y, z)$. We define the volumic Lagrangian L energy for the two-phase system using the classical expression

$$L(\rho, \mathbf{j}, y, z) = \frac{1}{2}\rho|\mathbf{u}|^2 - \rho f(\rho, y, z) = \frac{1}{2}\frac{|\mathbf{j}|^2}{\rho} - \rho f(\rho, y, z). \quad (1)$$

Finally, we also suppose that the global density verifies the continuity equation

$$\frac{\partial \rho}{\partial t} + \operatorname{div}(\rho\mathbf{u}) = 0. \quad (2)$$

2.2 Lagrangian Action Minimization

We consider the transformation between two instants $t_1 < t_2$ of a volume of fluid which initially occupies a volume represented by an open subset $\Omega(0)$ of \mathbb{R}^d ($d = 1, 2, 3$).

From an Eulerian point of view, according to our assumptions concerning the state variables, the transformations that act on this volume of fluid are known as soon as we know the map $(x, t) \mapsto (\rho, \mathbf{j}, y, z)(x, t)$, where x denotes the Eulerian space variable. From the Lagrangian point of view, if X denotes the lagrangian material reference coordinate, the transformations acting on $\Omega(0)$ are known as soon as we know the map $(X, t) \mapsto (x = \chi, y, z)$ where χ is \mathcal{C}^1 -diffeomorphism and the velocity is defined by $\mathbf{u}(\chi(X, t), t) = (\partial\chi/\partial t)_X(\chi(X, t), t)$. Within this framework, $(X, t) \mapsto \chi$ describes the fluid particles trajectories, while $(X, t) \mapsto y$ and $(X, t) \mapsto z$ are two fields associated with the fluid particles.

Let us now consider a family of transformations expressed in Lagrangian form $(X, t, \nu) \mapsto (\hat{x} = \hat{\chi}, \hat{y}, \hat{z})(X, t, \nu)$ parametrized by a real coefficient ν and the matching Eulerian family of transformations $(\hat{x}, t, \nu) \mapsto (\hat{\rho}, \hat{\mathbf{j}}, \hat{y}, \hat{z})(\hat{x}, t, \nu)$. We note $\hat{\Omega}(t, \nu)$ the image of $\Omega(0)$ by $\hat{\chi}(\cdot, t, \nu)$ (see figure 1), namely

$$\hat{\Omega}(t, \nu) = \{\hat{\chi}(X, t, \nu) / X \in \Omega(0)\},$$

We add the following classical assumptions:

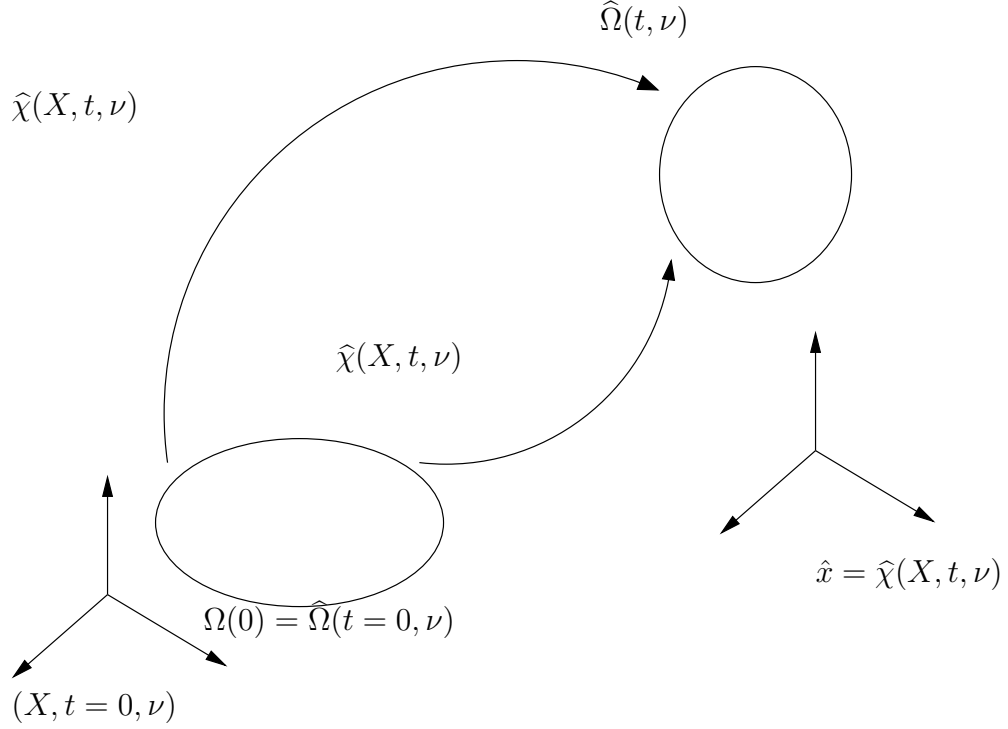


Figure 1: ν parametrized family of transformations $\hat{\chi}$.

- $\hat{\chi}$ is \mathcal{C}^1 -diffeomorphism and the velocity is defined by

$$\hat{\mathbf{u}}\left(\hat{\chi}(X, t), t, \nu\right) = \left(\frac{\partial \hat{\chi}}{\partial t}\right)_{X, \nu} \left(\hat{\chi}(X, t, \nu), t, \nu\right),$$

- for a given ν the density function $(\hat{x}, t) \mapsto \hat{\rho}(\hat{x}, t, \nu)$ verifies the mass conservation, *i.e.* for all $t \in (t_1, t_2)$

$$\int_{\Omega(0)} \rho(X, 0) dX = \int_{\hat{\Omega}(\nu, t)} \hat{\rho}(\hat{x}, t, \nu) d\hat{x},$$

- for all $X \in \Omega(0)$ and all $t \in (t_1, t_2)$

$$(\hat{\chi}, \hat{y}, \hat{z})(X, t, \nu = 0) = (\chi, y, z)(X, t),$$

- for all $X \in \partial\Omega(0)$, $t \in (t_1, t_2)$ and all ν

$$(\hat{\chi}, \hat{y}, \hat{z})(X, t, \nu) = 0.$$

The Lagrangian action $\mathcal{A}(\nu)$ associated with $\hat{\Omega}$ between the instants $t_1 < t_2$ reads

$$\mathcal{A}(\nu) = \int_{t_1}^{t_2} \int_{\hat{\Omega}(t, \nu)} L(\hat{\rho}, \hat{\mathbf{j}}, \hat{y}, \hat{z})(\hat{x}, t, \nu) d\hat{x} dt,$$

in order to use the Least Action principle, we need to compute $(d\mathcal{A}/d\nu)(\nu = 0)$. Supposing enough regularity so that differentiating is allowed under the integral sign we have

$$\begin{aligned} \frac{d\mathcal{A}}{d\nu}(\nu) = \int_{t_1}^{t_2} \int_{\hat{\Omega}(t,\nu)} & \left[\frac{\partial L}{\partial \mathbf{j}} \left(\frac{\partial \hat{\mathbf{j}}}{\partial \nu} \right)_{\hat{x},t} + \frac{\partial L}{\partial \rho} \left(\frac{\partial \hat{\rho}}{\partial \nu} \right)_{\hat{x},t} + \frac{\partial L}{\partial y} \left(\frac{\partial \hat{y}}{\partial \nu} \right)_{\hat{x},t} + \frac{\partial L}{\partial z} \left(\frac{\partial \hat{z}}{\partial \nu} \right)_{\hat{x},t} \right] d\hat{x} dt \\ & + \int_{t_1}^{t_2} \int_{\partial \hat{\Omega}(t,\nu)} L(\hat{\rho}, \hat{\mathbf{j}}, \hat{y}, \hat{z}) \hat{\mathbf{n}} \cdot \left(\frac{\partial \hat{x}}{\partial \nu} \right)_{X,t} d\hat{\sigma} dt. \end{aligned}$$

According to our hypotheses the boundary term vanishes and we thus have

$$\delta \mathcal{A} = \frac{d\mathcal{A}}{d\nu}(0) = \int_{t_1}^{t_2} \int_{\hat{\Omega}(t,0)} \left\{ \frac{\partial L}{\partial \mathbf{j}} \delta \mathbf{j} + \frac{\partial L}{\partial \rho} \delta \rho + \frac{\partial L}{\partial y} \delta y + \frac{\partial L}{\partial z} \delta z \right\} dx dt, \quad (3)$$

where

$$\begin{aligned} \delta \rho(x, t) &= \left(\frac{\partial \hat{\rho}}{\partial \nu} \right)_{\hat{x},t} (x, t, \nu = 0), & \delta \mathbf{j}(x, t) &= \left(\frac{\partial \hat{\mathbf{j}}}{\partial \nu} \right)_{\hat{x},t} (x, t, \nu = 0), \\ \delta y(x, t) &= \left(\frac{\partial \hat{y}}{\partial \nu} \right)_{\hat{x},t} (x, t, \nu = 0), & \delta z(x, t) &= \left(\frac{\partial \hat{z}}{\partial \nu} \right)_{\hat{x},t} (x, t, \nu = 0). \end{aligned}$$

If we define ξ the virtual displacement by

$$\xi(X, t) = \left(\frac{\partial \hat{x}}{\partial \nu} \right)_{X,t} (X, t, \nu = 0),$$

then we see that δy and δz are arbitrary, while $\delta \rho$ and $\delta \mathbf{j}$ are to be connected with ξ .

Our choice of the parametered transformations family involves the physical time t and the parameter ν as two identical variable, which means that what is available for t is also available for ν . More precisely, using the mass conservation ansatz, we have for a given ν and $t \in (t_1, t_2)$

$$\int_{\Omega(0)} \rho(X, 0) dX = \int_{\hat{\Omega}(\nu,t)} \rho(\hat{x}, t, \nu) d\hat{x} = \int_{\Omega(0)} \rho(\hat{\chi}(X, t, \nu), t, \nu) \left| \det \left(\frac{\partial \hat{\chi}}{\partial X} \right) \right| dX,$$

which equivalently reads

$$\rho(X, 0) = \rho(\hat{\chi}(X, t, \nu), t, \nu) \left| \det \left(\frac{\partial \hat{\chi}}{\partial X} \right) \right|.$$

In the above classical relation, we see that the role of t and ν are absolutely symmetric, which allows us to write a mass conservation according to the variation in ν , namely

$$\left(\frac{\partial \hat{\rho}}{\partial \nu} \right)_{\hat{x},t} + \sum_i \frac{\partial}{\partial \hat{x}_i} \left[\hat{\rho} \left(\frac{\partial \hat{x}_i}{\partial \nu} \right)_{X,t} \right] = 0.$$

The previous relation gives immediately for $\nu = 0$

$$\delta\rho = -\operatorname{div}(\rho\xi). \quad (4)$$

We now turn to the expression of $\delta\mathbf{u}$. This time, what comes into play is the simple assumptions that the Lagrangian and the Eulerian transformations family are connected. Indeed, using the definition of the velocity $\hat{\mathbf{u}}$, we have by the chain rule

$$\left(\frac{\partial\hat{\mathbf{u}}}{\partial\nu}\right)_{X,t} = \frac{\partial}{\partial\nu}\left(\hat{\mathbf{u}}[\hat{\chi}(X,t,\nu),t,\nu]\right) = \left(\frac{\partial\hat{\mathbf{u}}}{\partial\nu}\right)_{\hat{x},t} + \left(\frac{\partial\hat{\mathbf{u}}}{\partial\hat{x}}\right)_{\nu,t} \left(\frac{\partial\hat{\chi}}{\partial\nu}\right)_{X,t}. \quad (5)$$

But the definition of $\hat{\mathbf{u}}$ also implies that

$$\left(\frac{\partial\hat{\mathbf{u}}}{\partial\nu}\right)_{X,t} = \frac{\partial^2\hat{\chi}}{\partial\nu\partial t},$$

which reads for $\nu = 0$

$$\left(\frac{\partial\hat{\mathbf{u}}}{\partial\nu}\right)_{X,t}(X,t,\nu=0) = \left(\frac{\partial\xi}{\partial t}\right)_X(X,t) = \frac{d\xi}{dt}(x,t),$$

where $d/dt = \partial/\partial t + \mathbf{u} \cdot \nabla$ is the material derivative. Taking $\nu = 0$ in (5) and using the above relation provides finally

$$\delta\mathbf{u} = \frac{d\xi}{dt} - \frac{\partial\mathbf{u}}{\partial x}\xi.$$

As $\delta\mathbf{j} = \rho\delta\mathbf{u} + \mathbf{u}\delta\rho$, we deduce from (4) that

$$\delta\mathbf{j} = \frac{\partial}{\partial t}(\rho\xi) + \operatorname{div}(\xi \otimes \mathbf{j} - \mathbf{j} \otimes \xi), \quad (6)$$

where for any vector $\mathbf{a} = (a_i)_i$ and $\mathbf{b} = (b_i)_i$, $\operatorname{div}(\mathbf{a} \otimes \mathbf{b})$ is a vector defined by

$$\operatorname{div}(\mathbf{a} \otimes \mathbf{b})_i = \sum_j \frac{\partial(a_i b_j)}{\partial x_j}.$$

We now turn back to the Lagrangian action variation $\delta\mathcal{A}$. The Least Action Principle states that $\delta\mathcal{A} = 0$. Integrating by parts in (3) together with (4) and (6) provides

$$\begin{aligned} \delta\mathcal{A} = & \int_{t_1}^{t_2} \int_{\hat{\Omega}(t,0)} \left\{ -\rho \frac{\partial\mathbf{u}}{\partial t} - (\nabla \times \mathbf{u}) \times \mathbf{j} + \rho \nabla \left(\frac{\partial L}{\partial \rho} \right) \right\} \cdot \xi \, dx \, dt \\ & + \int_{t_1}^{t_2} \int_{\hat{\Omega}(t,0)} \left\{ \frac{\partial L}{\partial z} \right\} \delta z \, dx \, dt + \int_{t_1}^{t_2} \int_{\hat{\Omega}(t,0)} \left\{ \frac{\partial L}{\partial y} \right\} \delta y \, dx \, dt. \end{aligned}$$

Since the above relation is true for arbitrary ξ , δz and δy , we deduce the three following relations

$$\rho \frac{\partial\mathbf{u}}{\partial t} + (\nabla \times \mathbf{u}) \times \mathbf{j} - \rho \nabla \left(\frac{\partial L}{\partial \rho} \right) = 0, \quad \frac{\partial L}{\partial z} = 0, \quad \frac{\partial L}{\partial y} = 0, \quad (7)$$

which provides the equation for the impulsion

$$\frac{\partial(\rho\mathbf{u})}{\partial t} + \operatorname{div}(\rho\mathbf{u} \otimes \mathbf{u}) - \operatorname{div} \left[\left(\rho|\mathbf{u}|^2 + \rho \left(\frac{\partial L}{\partial \rho} \right) \right) \mathbf{Id} \right] + \operatorname{div}(L\mathbf{Id}) = 0. \quad (8)$$

The motion equation (8) has been obtained with a general free energy f and in the next section, we shall exhibit a specific free energy that will be used for modelling work.

2.3 Free Energy Choice

In the following, we will note f_α , g_α and P_α respectively the free energy, the free enthalpy (or Gibbs enthalpy) and the pressure of the phase α . In the case of an isothermal process, these quantities only depend on ρ_α and are connected by

$$P_\alpha = \rho_\alpha^2 \frac{df_\alpha}{d\rho_\alpha}, \quad \frac{dP_\alpha}{d\rho_\alpha} = \rho_\alpha \frac{dg_\alpha}{d\rho_\alpha}, \quad (9)$$

which also read in terms of the volumic free energy $F_\alpha = \rho_\alpha f_\alpha$

$$g_\alpha = \frac{dF_\alpha}{d\rho_\alpha}, \quad P_\alpha = \rho_\alpha \frac{dF_\alpha}{d\rho_\alpha} - F_\alpha. \quad (10)$$

We now postulate the following expression for f

$$\rho f = \sum_{\alpha} \rho_{\alpha} z_{\alpha} f_{\alpha}, \quad (11)$$

where f_α is the free energy of the α phase. We are now able to detail the term $(\partial L / \partial \rho)$ using relations (9), we have

$$\rho \left(\frac{\partial L}{\partial \rho} \right) = -\frac{1}{2} \rho |\mathbf{u}|^2 - \rho f - \sum_{\alpha} z_{\alpha} P_{\alpha}.$$

The above relation combined with (8) gives

$$\partial_t(\rho\mathbf{u}) + \operatorname{div}(\rho\mathbf{u} \otimes \mathbf{u}) + \operatorname{div}(P\mathbf{Id}) = 0, \quad (12)$$

where P is a generalized pressure given by

$$P = \sum_{\alpha} z_{\alpha} P_{\alpha}. \quad (13)$$

Finally, the last two expressions of relation (7), namely $\partial L / \partial z = 0$ and $\partial L / \partial y = 0$ respectively read now $P_1 - P_2 = 0$ and $g_1 - g_2 = 0$. We shall see that both of these relations express the conservative aspect of the system we just derived. The lack of dissipative mechanisms is a consequence of the Lagrangian formalism. Let us also note that this formalism has not provided any additional data related to the equation verified by z nor y . This means that the Lagrangian structure we chose here does not embed any conservative processes acting on y or z .

In the next section we will show how to prescribe such mechanisms by the mean of an entropy inequality.

2.4 Dissipative Structures

As the isothermal single-phase Euler system, we choose $[\rho f + \rho|\mathbf{u}|^2/2, (\rho f + \rho|\mathbf{u}|^2/2 + P)\mathbf{u}]$ as the (mathematical) entropy-entropy flux pair associated with our system. We shall see that it is possible to design an entropy inequality based on this pair, by solely prescribing effects connected to the evolution of y and z , neglecting any other dissipation source such as viscosity.

Using the mass conservation (2) and the impulsion equation (12), this leads to

$$\partial_t \left(\rho f + \rho \frac{|\mathbf{u}|^2}{2} \right) + \operatorname{div} \left[\left(\rho f + \rho \frac{|\mathbf{u}|^2}{2} + P \right) \mathbf{u} \right] = \rho(g_1 - g_2) \frac{dy}{dt} + (P_2 - P_1) \frac{dz}{dt}.$$

For the above relation to be an inequality, we need the dissipation rate $\rho(g_1 - g_2)dy/dt + (P_2 - P_1)dz/dt$ to be a signed quantity. This suggests two simple closure relations involving y and z

$$\rho \frac{dy}{dt} = \lambda(g_2 - g_1), \quad \frac{dz}{dt} = \kappa(P_1 - P_2), \quad (14)$$

where λ and κ are non negative parameters. Such choice enables the entropy to verify the following equation

$$\partial_t \left(\rho f + \rho \frac{|\mathbf{u}|^2}{2} \right) + \operatorname{div} \left[\left(\rho f + \rho \frac{|\mathbf{u}|^2}{2} + P \right) \mathbf{u} \right] = -\lambda(g_1 - g_2)^2 - \kappa(P_1 - P_2)^2 \leq 0,$$

and imposes y and z to be governed by the relations (14).

3 System Properties

This section is devoted to the study of the basic properties of the system derived in section 2, which reads

$$\begin{cases} \partial_t(\rho_1 z_1) + \operatorname{div}(\rho_1 z_1 \mathbf{u}) = \lambda[g_2(\rho_2) - g_1(\rho_1)], \\ \partial_t(\rho_2 z_2) + \operatorname{div}(\rho_2 z_2 \mathbf{u}) = -\lambda[g_2(\rho_2) - g_1(\rho_1)], \\ \partial_t(\rho \mathbf{u}) + \operatorname{div}(\rho \mathbf{u} \otimes \mathbf{u} + P \operatorname{Id}) = 0, \\ \partial_t z + \mathbf{u} \cdot \nabla z = \kappa[P_1(\rho_1) - P_2(\rho_2)], \end{cases} \quad (15)$$

where $P = zP_1(\rho_1) + (1 - z)P_2(\rho_2)$. In the following, this system will be referred to as the relaxed system.

3.1 Relaxed System

Considering smooth solutions $\mathbf{V} = (\rho_1 z_1, \rho_2 z_2, \rho u, z)^T$, the system (15) is equivalent for one-dimensional problems to the quasilinear formulation

$$\partial_t \mathbf{V} + A(\mathbf{V}) \partial_x \mathbf{V} = \mathcal{R}(\mathbf{V}),$$

with

$$\mathcal{R}(\mathbf{V}) = \begin{bmatrix} \lambda(g_2 - g_1) \\ -\lambda(g_2 - g_1) \\ \kappa(P_1 - P_2) \end{bmatrix}, \quad \mathbf{A}(\mathbf{V}) = \begin{bmatrix} uy_2 & -uy_1 & y_1 & 0 \\ -uy_2 & uy_1 & y_2 & 0 \\ c_1^2 - u^2 & c_2^2 - u^2 & 2u & M \\ 0 & 0 & 0 & u \end{bmatrix}. \quad (16)$$

The quantity $c_\alpha^2 = dP_\alpha/d\rho_\alpha$ is the squared sound velocity of phase $\alpha = 1, 2$ and $M = \partial P/\partial z$. Denoting by c the mixture sound velocity defined by

$$c^2 = \sum_{\alpha} y_{\alpha} c_{\alpha}^2,$$

the matrix $A(\mathbf{V})$ possesses four eigenvalues $\Lambda_1 = u - c$, $\Lambda_2 = \Lambda_3 = u$ and $\Lambda_4 = u + c$. The corresponding left and right eigenvectors \mathbf{l}_k and \mathbf{r}_k , $k = 1, \dots, 4$ are defined by

$$(\mathbf{l}_1, \mathbf{l}_2, \mathbf{l}_3, \mathbf{l}_4) = \frac{1}{2c^2} \begin{bmatrix} c_1^2 + uc & -2y_1c_1^2 + 2c^2 & -2y_2c_1^2 & c_1^2 - uc \\ c_2^2 + uc & -2y_1c_2^2 & 2c^2 - 2y_2c_2^2 & c_2^2 - uc \\ -c & 0 & 0 & c \\ M & -2y_1M & -2y_2M & M \end{bmatrix}, \quad (17)$$

$$(\mathbf{r}_1, \mathbf{r}_2, \mathbf{r}_3, \mathbf{r}_4) = \begin{bmatrix} y_1 & 1 & 0 & y_1 \\ y_2 & 0 & 1 & y_2 \\ u - c & u & u & u + c \\ 0 & -c_1^2/M & c_2^2/M & 0 \end{bmatrix}. \quad (18)$$

This set of eigenvectors verifies the classical orthogonality property: $\mathbf{l}_i \cdot \mathbf{r}_j = 0$ for $i \neq j$ and $\mathbf{l}_i \cdot \mathbf{r}_j = 1$ for $i = j$.

This eigenstructure shows that the system (15) is hyperbolic. Nevertheless the entropy of the system is not strictly convex. Indeed, there is a loss of convexity in the z direction, therefore the entropy-entropy flux pair we used here does not provide any information about the symmetrizability of the system (15).

Let us finally note that the fields associated with the 1-wave and the 4-wave are genuinely non-linear while the fields associated with the 2-wave and the 3-wave are linearly degenerate. The latter ensures that for a weak solution of the system (15) without source terms, u and z cannot jump simultaneously. In that sense, the non-conservative product $\mathbf{u} \cdot \nabla z$ is well defined for system (15), as well as the Rankine-Hugoniot jump relations across a discontinuity.

Remark 1. The equation for z in (15) is equivalent to the following balance equation

$$\partial_t(\rho z) + \operatorname{div}(\rho z \mathbf{u}) = \kappa \rho [P_1(\rho_1) - P_2(\rho_2)].$$

3.2 Limit System $\kappa = +\infty$, $\lambda < +\infty$ (M-equilibrium)

This limit system has been previously studied in [9]. We recall here some of the properties of the system.

The $\kappa = +\infty$ assumption in the system (15) is formally equivalent to compute $z \in [0, 1]$ such that

$$P_1\left(\frac{m_1}{z}\right) = P_2\left(\frac{m_2}{1-z}\right), \quad (19)$$

for given fixed values $m_1 = \rho_1 z_1 \geq 0$ and $m_2 = \rho_2 z_2 \geq 0$.

Proposition 3.1. [9] Suppose functions $\rho_\alpha \mapsto P_\alpha(\rho_\alpha)$ are $\mathcal{C}^1(\mathbb{R}^+)$, are strictly increasing on \mathbb{R}^+ and tend to $+\infty$ when $\rho_\alpha \rightarrow +\infty$, then, there exists a unique $\check{z}(m_1, m_2) \in [0, 1]$ solution of the equation (19). Moreover, $m_1 \mapsto \check{z}(m_1, m_2)$ is non-decreasing on \mathbb{R}^+ , $m_2 \mapsto \check{z}(m_1, m_2)$ is non-increasing on \mathbb{R}^+ and $(m_1, m_2) \mapsto \check{z}(m_1, m_2)$ is as regular as $\rho_\alpha \mapsto P_\alpha(\rho_\alpha)$, $\alpha = 1, 2$.

Proof. Let us define $\varphi : (0, 1) \rightarrow \mathbb{R}$, $\varphi(z) = P_1[m_1/z] - P_2[m_2/(1-z)]$. Hypothesis show us that $\varphi(z) \rightarrow +\infty$ when $z \rightarrow 0$ and $\varphi(z) \rightarrow -\infty$ when $z \rightarrow 1$. Moreover, the derivative of φ is given by

$$\frac{d\varphi}{dz} = -\frac{m_1}{z^2} \frac{dP_1}{d\rho_1} - \frac{m_2}{(1-z)^2} \frac{dP_2}{d\rho_2} < 0.$$

This provides existence and uniqueness for $\check{z} \in [0, 1]$. The regularity of \check{z} follows from the implicit function theorem.

Concerning the monotonicity of \check{z} , using the equation (19), we have

$$\frac{\partial \check{z}}{\partial m_1} = \frac{c_1^2/\check{z}}{c_1^2 m_1/\check{z}^2 + c_2^2 m_2/(1-\check{z})^2}, \quad \frac{\partial \check{z}}{\partial m_2} = -\frac{c_2^2/(1-\check{z})}{c_1^2 m_1/\check{z}^2 + c_2^2 m_2/(1-\check{z})^2},$$

which ends the proof. \square

Remark 2. Let us note that the proposition 3.1 is valid for $m_1 m_2 > 0$. However, when m_α , $\alpha = 1, 2$ reaches the bound of the states space, i.e. $m_1 = 0$ or $m_2 = 0$ then the meaning of the equation $P_1 = P_2$ becomes ambiguous and depends on the EOS used for the simulation. In practice, whenever $m_1 = 0$ (resp. $m_2 = 0$), we do not solve $P_1 = P_2$ anymore but use instead directly $P = P_2(\rho) = P_2(m_2)$ (resp. $P = P_1(\rho) = P_1(m_1)$).

Using \check{z} , the M-equilibrium system reads

$$\begin{cases} \partial_t(\rho_1 z_1) + \text{div}(\rho_1 z_1 \mathbf{u}) = \lambda[g_2(\rho_2) - g_1(\rho_1)], \\ \partial_t(\rho_2 z_2) + \text{div}(\rho_2 z_2 \mathbf{u}) = -\lambda[g_2(\rho_2) - g_1(\rho_1)], \\ \partial_t(\rho \mathbf{u}) + \text{div}(\rho \mathbf{u} \otimes \mathbf{u} + P \text{Id}) = 0, \end{cases} \quad (20)$$

with $P = P_1(\rho_1) = P_2(\rho_2) = \check{z}P_1 + (1-\check{z})P_2$.

Considering smooth solutions $\mathbf{W} = (\rho_1 z_1, \rho_2 z_2, \rho u)^T$ of (20), then the system (20) is equivalent in 1D to

$$\partial_t \mathbf{W} + B(\mathbf{W}) \partial_x \mathbf{W} = \mathcal{S}(\mathbf{W}),$$

where

$$\mathcal{S}(\mathbf{W}) = \begin{bmatrix} \lambda(g_2 - g_1) \\ -\lambda(g_2 - g_1) \\ 0 \end{bmatrix}, \quad B(\mathbf{W}) = \begin{bmatrix} u & 0 & \rho_1 z_1 \\ 0 & u & \rho_2 z_2 \\ (1/\rho)\partial_{m_1} P & (1/\rho)\partial_{m_2} P & u \end{bmatrix}.$$

The matrix $B(\mathbf{W})$ possesses three distinct eigenvalues $\check{\Lambda}_1 = u - \check{c}$, $\check{\Lambda}_2 = u$ and $\check{\Lambda}_3 = u + \check{c}$, where \check{c} is defined by

$$\frac{1}{\rho \check{c}^2} = \sum_{\alpha} \frac{\check{z}}{\rho_{\alpha} c_{\alpha}^2}.$$

This ensures the strict hyperbolicity of the system M-equilibrium (20).

Remark 3. A similar remark as the remark 2 can be expressed for the system (20) as the behavior of $g_\alpha(\rho_\alpha)$ may become ambiguous when $m_\alpha \rightarrow 0$, $\alpha = 1, 2$, depending on the EOS. In practice, we set $g_1 - g_2 = 0$ when $m_1 m_2 = 0$. Let us also underline that in practice, the numerical diffusion of the approximation schemes generates mixing zones where $m_1 m_2 > 0$, even if $m_1 m_2 = 0$ in the whole computational domain at the initial time.

3.3 Limit System $\kappa = +\infty$, $\lambda = +\infty$ (MT-equilibrium)

The condition $\kappa = +\infty$ and $\lambda = +\infty$ (MT-equilibrium) is formally equivalent to determine $m_1 \geq 0$, $m_2 \geq 0$ and $z \in [0, 1]$, for a given $\rho > 0$, such that

$$P_1\left(\frac{m_1}{z}\right) = P_2\left(\frac{m_2}{1-z}\right), \quad g_1\left(\frac{m_1}{z}\right) = g_2\left(\frac{m_2}{1-z}\right), \quad \rho = m_1 + m_2,$$

or equivalently, to find $\rho_1 \geq 0$, $\rho_2 \geq 0$ and $z \in [0, 1]$ such that for a given $\rho > 0$

$$P_1(\rho_1) = P_2(\rho_2), \quad g_1(\rho_1) = g_2(\rho_2), \quad \rho = z\rho_1 + (1-z)\rho_2. \quad (21)$$

Let us note that the above system does no longer depend on m_1 , m_2 and z but solely on the parameter ρ . Unfortunately, on the contrary of system (19), nor existence nor unicity for the solution of (21) is ensured. However, this issue seems natural. Indeed, it expresses the fact that it is not possible to prescribe a mass transfer mechanism between two fluids with two arbitrary EOS. A certain degree of compatibility between both fluids EOS is required in order to define correctly the thermodynamical equilibrium. Despite the lack of analytical solvability criterion for the system (21), we are able to give it a geometrical interpretation.

We recall that $F_\alpha = \rho_\alpha f_\alpha$ denotes the volumic free energy of the α phase. Considering the curves \mathcal{C}_α of the functions $\rho_\alpha \mapsto F_\alpha(\rho_\alpha)$, *i.e.* the graph of F_α in the (ρ, F) -plane and consider $\mathcal{D}_\alpha(\rho_\alpha)$ the tangent line to \mathcal{C}_α at the point $(\rho_\alpha, F_\alpha(\rho_\alpha))$. We see that $g_\alpha(\rho_\alpha)$ and $P_\alpha(\rho_\alpha)$ are respectively the slope and the F -intercept of the straight line $(\rho_\alpha, F_\alpha(\rho_\alpha))$. Consequently (ρ_1^*, ρ_2^*) is a solution of system $P_1 = P_2$ and $g_1 = g_2$ if and only if $\mathcal{D}_1(\rho_1^*)$ and $\mathcal{D}_2(\rho_2^*)$ have the same slope and same F -intercept, namely $\mathcal{D}_1(\rho_1^*) = \mathcal{D}_2(\rho_2^*)$. This geometrical construction of ρ_α^* , called the bi-tangent condition, is illustrated in the figure 2.

We now consider the case of stiffened gas EOS. For such fluids, the EOS are given by

$$P_\alpha = a_\alpha \rho_\alpha - P_\alpha^\infty, \quad g_\alpha = b_\alpha + a_\alpha \log(\rho_\alpha), \quad (22)$$

where the constants a_α and b_α are related to the constant flow temperature T as follows

$$\begin{cases} a_\alpha(T) = (\gamma_\alpha - 1)c_{v_\alpha}T, \\ b_\alpha(T) = q_\alpha + \left[\gamma_\alpha c_{v_\alpha} - q'_\alpha + (\gamma_\alpha - 1)c_{v_\alpha} \log [(\gamma_\alpha - 1)c_{v_\alpha}] - c_{v_\alpha} \log T \right] T. \end{cases}$$

Parameters $\gamma_\alpha > 1$, $P_\alpha^\infty \geq 0$, $c_{v_\alpha} > 0$, q_α and q'_α being constant for each fluid $\alpha = 1, 2$. For this particular EOS case, the bi-tangent condition is equivalent to the following analytical condition. Let us finally note that for a stiffened gas $c_\alpha^2 = a_\alpha$, $\alpha = 1, 2$.

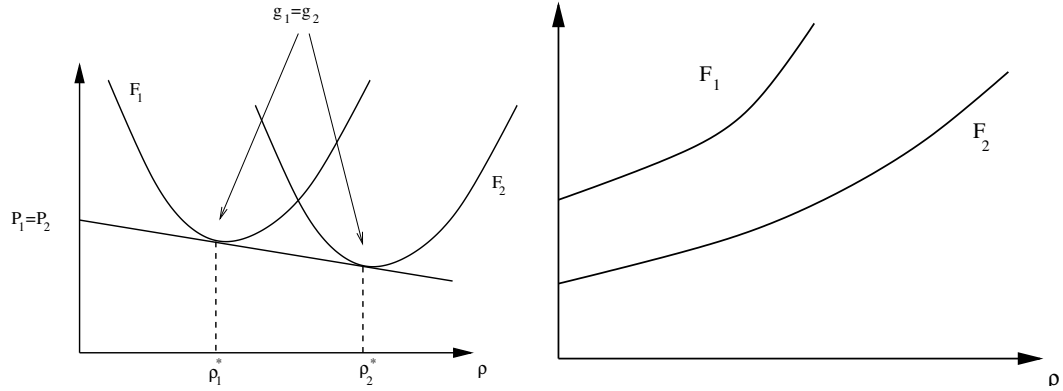


Figure 2: Examples of admissible EOS (left) and non-admissible EOS (right)

Proposition 3.2. For given stiffened gas EOS, (ρ_1^*, ρ_2^*) verifies $P_1(\rho_1) = P_2(\rho_2)$ and $g_1(\rho_1) = g_2(\rho_2)$ if

$$\begin{cases} \rho_2^* = (\rho_1^*)^{a_1/a_2} \exp\left(\frac{b_1 - b_2}{a_2}\right), \\ a_1 \rho_1^* + (P_1^\infty - P_2^\infty) - a_2 (\rho_1^*)^{a_1/a_2} \exp\left(\frac{b_1 - b_2}{a_2}\right) = 0. \end{cases} \quad (23)$$

If $(a_1 - a_2)(P_2^\infty - P_1^\infty) \geq 0$ then system (23) admits a unique solution, while if $(a_1 - a_2)(P_2^\infty - P_1^\infty) < 0$, it has two or no solution.

Remark 4. When considering perfect gas fluids, i.e. $P_\alpha^\infty = 0$, $q_\alpha = 0$, $q'_\alpha = 0$, an explicit relation for ρ_α^* is available

$$\rho_1^* = \exp\left(-\frac{b_1 - b_2}{a_1 - a_2}\right) \left(\frac{a_1}{a_2}\right)^{a_2/(a_1 - a_2)}, \quad \rho_2^* = \exp\left(-\frac{b_1 - b_2}{a_1 - a_2}\right) \left(\frac{a_1}{a_2}\right)^{a_1/(a_1 - a_2)}.$$

In the sequel, we shall always consider that there exists a unique solution (ρ_1^*, ρ_2^*) of system $P_1 = P_2$ and $g_1 = g_2$. Consequently, ρ_1^* and ρ_2^* will have fixed values which only depend on the fluids EOS definition. Up to a renumbering we suppose that $\rho_1^* < \rho_2^*$.

We now complete the construction of the equilibrium state solution of (21), by providing the value of $z^* \in [0, 1]$ solution of $\rho = z\rho_1^* + (1 - z)\rho_2^*$. We set

$$z^* = 1 \text{ if } \rho < \rho_1^*, \quad z^* = \frac{\rho - \rho_2^*}{\rho_1^* - \rho_2^*} \text{ if } \rho_1^* < \rho < \rho_2^*, \quad z^* = 0 \text{ if } \rho_2^* < \rho. \quad (24)$$

Finally, the MT-equilibrium system is formally equivalent to

$$\begin{cases} \partial_t \rho + \operatorname{div}(\rho \mathbf{u}) = 0, \\ \partial_t(\rho \mathbf{u}) + \operatorname{div}(\rho \mathbf{u} \otimes \mathbf{u} + P \operatorname{Id}) = 0, \end{cases} \quad (25)$$

with the pressure P determined by

$$P(\rho) = \begin{cases} P_1(\rho) & \text{if } z^* = 1, \\ z^* P_1(\rho_1^*) + (1 - z^*) P_2(\rho_2^*) & \text{if } z^* \in (0, 1), \\ P_2(\rho) & \text{if } z^* = 0. \end{cases} \quad (26)$$

The resulting pressure law $\rho \mapsto P(\rho)$ is continuously differentiable with the exception of points ρ_1^* and ρ_2^* where it is only continuous (see figure 3.3 for the profile of $\rho \mapsto P(\rho)$). System (25) has a structure close to the isothermal Euler equations, however, the system is only weakly hyperbolic. Indeed, for $\rho \notin \{\rho_1^*, \rho_2^*\}$, it is possible to compute the jacobian matrix associated with the system. It possesses two eigenvalues $\Lambda_1^* = u - c^*$ and $\Lambda_2^* = u + c^*$, where $(c^*)^2 = dP/d\rho$. While $c^* > 0$ for $\rho \notin [\rho_1^*, \rho_2^*]$, in the case $\rho \in (\rho_1^*, \rho_2^*)$, $c^* = 0$. In this case, both eigenvalues collapse and the system loses its eigenvector basis.

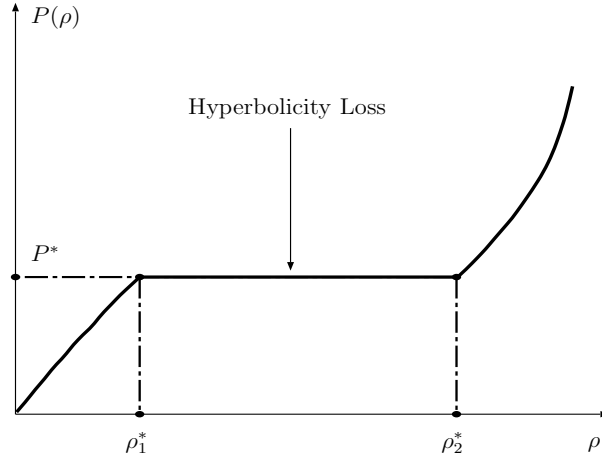


Figure 3: Profile of the pressure law $\rho \mapsto P(\rho)$.

A remarkable property of the resulting equilibrium system is that it complies with an entropy convexification argument.

Proposition 3.3. *Let us consider the subset E of the (ρ, F) -plane which is the union of the function $\rho_\alpha \mapsto \rho_\alpha f_\alpha(\rho_\alpha)$ epigraphs, namely*

$$E = \{(\rho, F) \in (\mathbb{R}_+)^2 / F \geq \rho \min[f_1(\rho), f_2(\rho)]\}.$$

Let \mathcal{C} be the convex hull of E and let F be the function whose epigraph is \mathcal{C} . By definition F is (weakly) convex, $F + \rho|\mathbf{u}|^2/2$ is an entropy for the system (25) and the pressure P in (26) is defined by $P = dF/d\rho - F$.

This convexification property has been previously used within the broader context of anisothermal flows by S. Jaouen in [16] as a design principle. The key idea was to break down the spinodal zone in a fluid EOS by replacing it with a convexified surface. In this way, the system (25)–(26) coincide with the models derived by S. Jaouen when considering isothermal flows. Let us also underline that the loss of hyperbolicity is a pathology that seems only to affect the present isothermal models.

Remark 5. Within the present formalism, the equilibrium pressure law given by (26) when $z^ \notin \{0, 1\}$ can be interpreted as the saturation pressure and depends solely on the temperature T .*

Remark 6. The solution of the Riemann problem for the MT-equilibrium system may not be unique in the class of weak entropic solutions. In this sense, the system is not well-posed in this class of solutions.

3.4 Connection with the Van der Waals Equation of States

In this section we explore the connection between the equilibrium states of the Van der Waals EOS and the MT-equilibrium system.

The volumic free energy for the Van der Waals reads

$$F(\rho) = \rho f(\rho) = -a\rho^2 - RT\rho \ln\left(\frac{1}{\rho} - b\right),$$

which gives the well-known Van der Waals pressure law

$$P(\rho) = \rho^2 \frac{df}{d\rho}(\rho) = \frac{\rho RT}{1 - b\rho} - a\rho^2,$$

where R , a and b are positive constants. As we only consider isothermal transformations, we did not use the temperature T as a variable but as a parameter of the EOS. We suppose that the temperature is below the critical temperature, namely $T < \frac{8a}{27Rb}$. Figure 4 depicts the behavior of $\rho \mapsto P(\rho)$ and $\rho \mapsto F(\rho)$ for such temperature values. Let us recall the definition of the Maxwell points below the critical

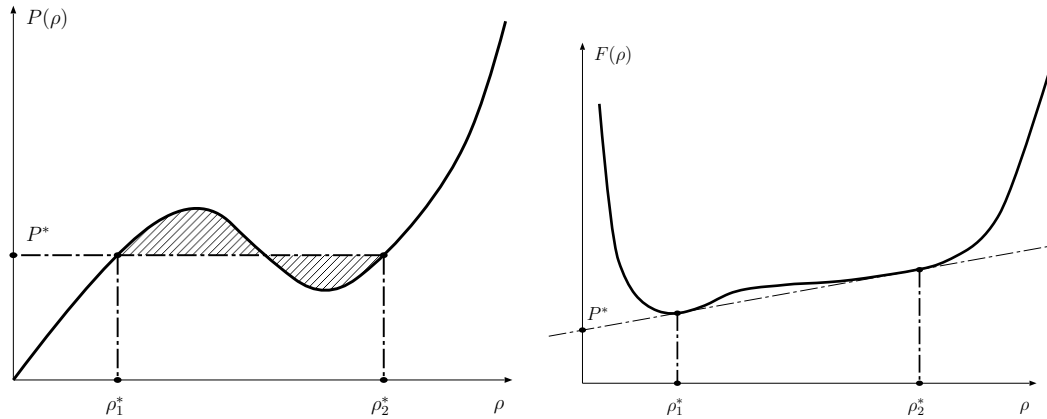


Figure 4: Graph of the (P, ρ) and (F, ρ) isotherms for the Van der Waals EOS.

temperature: there exist two values ρ_1^* and ρ_2^* such that

$$g(\rho_1^*) = g(\rho_2^*), \quad P(\rho_1^*) = P(\rho_2^*) = P^*. \quad (27)$$

Two interpretations of relation (27) are available. In the (P, ρ) -plane, equation (27) corresponds with the definition of the Maxwell points: (ρ_1^*, P^*) and (ρ_2^*, P^*) cut the graph of the (P, ρ) isotherm such that both hatched areas displayed on figure 4 are equal. Another equivalent standpoint uses the graph of the isotherm in the (F, ρ) -plane: the line defined by (ρ_1^*, P^*) and (ρ_2^*, P^*) is the bi-tangent to the isotherm

graph. As seen previously, the slope of the bi-tangent line is $g(\rho_1^*) = g(\rho_2^*)$ and its F -intercept is P^* .

The definition of the equilibria can also be expressed within both (P, ρ) and (F, ρ) framework. In the (P, ρ) -plane, the equilibrium points of the Van der Waals equation verifies the relation $\rho \mapsto P^{\text{eq}}(\rho)$, where

$$P^{\text{eq}}(\rho) = \begin{cases} P(\rho), & \text{if } \rho < \rho_1^*, \\ P^*, & \text{if } \rho_1^* \leq \rho \leq \rho_2^*, \\ P(\rho), & \text{if } \rho_2^* < \rho. \end{cases}$$

In the F - v plane, the equilibrium points comply with the EOS $\rho \mapsto F^{\text{eq}}(\rho)$, where the graph of $\rho \mapsto F^{\text{eq}}(\rho)$ is the convex hull of the graph of $\rho \mapsto F(\rho)$.

Proposition 3.4. *There exist two EOS $\rho_\alpha \mapsto F_\alpha(\rho_\alpha)$, $\alpha = 1, 2$ such that the MT-equilibrium system associated with the fluids governed by F_1 and F_2 is the equilibrium system of the Van der Waals EOS. Moreover, there is an infinity of possible choices for F_1 and F_2 .*

Proof. Let \mathcal{C}_{vdw} be the graph of $\rho \mapsto F(\rho)$ where F is the free energy of Van der Waals. Consider a smooth strictly convex curve \mathcal{C}_1 (resp. \mathcal{C}_2) that coincides with $\rho \mapsto F(\rho)$ for $\rho < \rho_1^*$ (resp. $\rho_2^* < \rho$) and that is tangential to \mathcal{C}_1 (resp. \mathcal{C}_2) at $\rho = \rho_1^*$ (resp. $\rho = \rho_2^*$) as depicted on figure 5. It is straightforward that union of \mathcal{C}_1 epigraph and \mathcal{C}_2 epigraph has the same convex hull as \mathcal{C}_{vdw} . Therefore if \mathcal{C}_α is the graph of $\rho_\alpha \mapsto F_\alpha(\rho_\alpha)$, $\alpha = 1, 2$ then the MT-equilibrium system associated with F_1 and F_2 is the equilibrium system associated with the Van der Waals EOS. \square

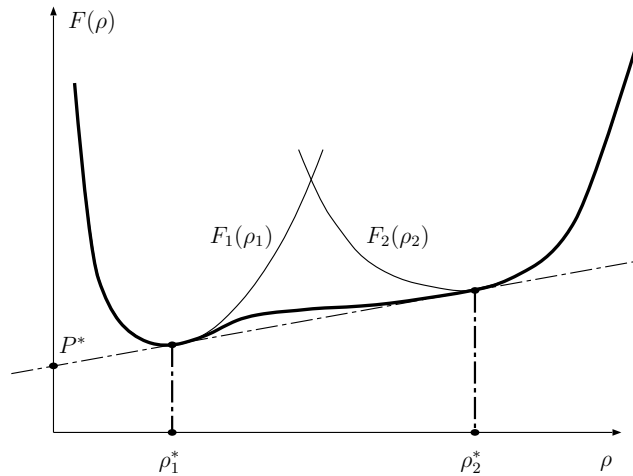


Figure 5: Graph of two EOS in the (F, ρ) -plane whose MT-equilibrium is the equilibrium of the Van der Waals EOS.

4 Numerical Treatment

From now on, we shall suppose that both fluids are governed by a stiffened gas EOS. The numerical schemes are presented within a 1D framework. For the 2D tests we implemented a classical directionnal splitting strategy.

Consider $i \in \mathbb{Z}$, $n \in \mathbb{N}$ and let $\Delta x > 0$ and $\Delta t > 0$ be the space and time steps. Recalling that $\mathbf{W} = (\rho_1 z_1, \rho_2 z_2, \rho u)^T$, we note \mathbf{W}_i^n and z_i^n the finite volume approximation of \mathbf{W} and z in the cell i at the instant $t_n = n\Delta t$

$$\mathbf{W}_i^n \simeq \frac{1}{\Delta x} \int_{(i-1/2)\Delta x}^{(i+1/2)\Delta x} \mathbf{W}(x, t_n) dx, \quad z_i^n \simeq \frac{1}{\Delta x} \int_{(i-1/2)\Delta x}^{(i+1/2)\Delta x} z(x, t_n) dx.$$

The numerical strategy we adopt here is a classical two-step scheme which consists in a first convective step thanks to a discretization of the source terms free relaxed system (15)

$$\begin{cases} \mathbf{W}_i^{n+1/2} = \mathbf{W}_i^n - \frac{\Delta t}{\Delta x} [\mathbf{G}_{i+1/2}(\mathbf{W}^n, z^n) - \mathbf{G}_{i-1/2}(\mathbf{W}^n, z^n)], \\ z_i^{n+1/2} = z_i^n - \frac{\Delta t}{\Delta x} \mathbf{H}_i(\mathbf{W}^n, z^n), \end{cases} \quad (28)$$

followed by a projection (or relaxation) step onto the equilibrium states

$$(\mathbf{W}^{n+1}, z^{n+1}) = \Pi(\mathbf{W}^{n+1/2}, z^{n+1/2}).$$

The choice of a non-conservative scheme for z complies with the numerical techniques presented in [1, 2] for the five-equation model. This choice is also a simple mean that ensures a discrete maximum principle for z during the advection step.

Remark 7. The discretization of the equation for z is absolutely not necessary for solving the MT-equilibrium system as the projection step destroys the value $z^{n+1/2}$. Nevertheless we chose to keep this evolution step from z^n to $z^{n+1/2}$ in the present algorithm. This allows to switch from the MT-equilibrium system to the M-equilibrium system depending on whether the projection step is performed or not.

4.1 Numerical Scheme for the Convective Part

Following a similar approach as in [2] and [9], we shall use an upwind scheme for operator $H_i(\mathbf{W}^n, z^n)$ while the numerical flux operator $\mathbf{G}_{i+1/2}$ will be derived using a Roe-type linearization.

4.1.1 Roe-Type Linearization

Recall that $\mathbf{V} = (\mathbf{W}, z)$ and let us consider two constant states \mathbf{V}_L and \mathbf{V}_R , respectively on the left and right of the interface $i + 1/2$. Let us recall classical notations : for any vector or scalar a quantity, we note

$$\Delta a = a_R - a_L, \quad \bar{a} = \frac{\sqrt{\rho_L} a_L + \sqrt{\rho_R} a_R}{\sqrt{\rho_L} + \sqrt{\rho_R}}, \quad \underline{a} = \frac{\sqrt{\rho_L} a_R + \sqrt{\rho_R} a_L}{\sqrt{\rho_L} + \sqrt{\rho_R}}.$$

Our goal here is to define the vector \mathbf{R} such that

$$\mathbf{G}_{i+1/2}(\mathbf{W}^n, z^n) = \mathbf{G}(\mathbf{W}_i^n, z_i^n, \mathbf{W}_{i+1}^n, z_{i+1}^n),$$

$$\mathbf{G}(\mathbf{V}_L, \mathbf{V}_R) = \frac{1}{2} \begin{bmatrix} z_1 \rho_1 u \\ z_2 \rho_2 u \\ \rho u^2 + P \end{bmatrix}_L + \frac{1}{2} \begin{bmatrix} z_1 \rho_1 u \\ z_2 \rho_2 u \\ \rho u^2 + P \end{bmatrix}_R - \frac{1}{2} \mathbf{R}(\mathbf{V}_L, \mathbf{V}_R).$$

Let us consider a matrix A^* that we choose to be some average of $A(\mathbf{V}_L)$ and $A(\mathbf{V}_R)$ the values of the Jacobian matrix defined by relation (16) in section 3.1 taken at the states \mathbf{V}_L and \mathbf{V}_R . The form of A^* ensures that this matrix is diagonalizable.

Additionally, as for a classical Roe linearization we require A^* to satisfy a jump relation (see [21]). Since, system (15) is not in conservative form, one cannot impose the usual jump condition. Rather, A^* must satisfy a weak form of the Roe jump condition

$$\begin{bmatrix} \Delta(\rho_1 z_1 u) \\ \Delta(\rho_2 z_2 u) \\ \Delta(\rho u^2 + P) \\ u^* \Delta z \end{bmatrix} = A^*(\mathbf{V}_R - \mathbf{V}_L). \quad (29)$$

The relation (29) is based on the Rankine-Hugoniot relations that are available for the system (15) without source terms. The jump relation (29) is expressed in terms of the quasi-conservative variables $\mathbf{V} = (\mathbf{W}, z)$ instead of the conservative variables $(\mathbf{W}, \rho z)$ which should be used in a classical Roe scheme approach. Let us once again emphasize that the jump relation used in (29) is unambiguously valid as z and u cannot jump simultaneously.

We have the following property for the parameters that define A^* .

Proposition 4.1. *If one defines u^* , y_α^* and ρ^* by*

$$u^* = \bar{u}, \quad \rho^* = \bar{\rho} \quad \text{and} \quad y_\alpha^* = \bar{y}_\alpha, \quad (30)$$

and if there exists $(c_\alpha)^2$ and M^ such that the following discrete jump condition is verified*

$$\Delta P = \sum_{\alpha} (c_\alpha^2)^* \Delta(\rho_\alpha z_\alpha) + M^* \Delta z, \quad (31)$$

then the Roe matrix A^ defined with the above parameters verifies the jump condition (29).*

4.1.2 Numerical scheme

We now assume that we have a matrix A^* whose coefficient complies with the condition of proposition 4.1. We shall note $(\Lambda_j^*)_{j=1,\dots,4}$, $(\mathbf{r}_j^*)_{j=1,\dots,4}$ and $(\mathbf{l}_j^*)_{j=1,\dots,4}$ respectively the eigenvalues of A^* , the corresponding right and left eigenvectors basis defined by relations (17)–(18). Recall that the usual Roe numerical flux is given by $|A^*| \Delta \mathbf{V}$. In our case, we only keep its first three components denoted by $\mathbf{R}(\mathbf{V}_L, \mathbf{V}_R)$. More precisely, for $1 \leq k \leq 3$, the k th component of \mathbf{R} is given by

$$\mathbf{R}_k = (|A^*| \Delta \mathbf{V})_k = \sum_{j=1}^4 |\Lambda_j^*| \beta_j^*(\mathbf{r}_j^*)_k \quad k = 1, 2, 3, \quad (32)$$

where $\beta_j^* = \mathbf{1}_j^* \cdot \Delta \mathbf{V}$.

The jump relation (31) along with some basic algebra provide that β_j^* verify

$$\begin{cases} \beta_1^* = \frac{1}{2(c^*)^2} [\Delta P - \underline{\rho} c^* \Delta u], \\ \beta_2^* = \frac{1}{(c^*)^2} [-\bar{y}_1 \Delta P + (c^*)^2 \Delta(\rho_1 z_1)], \\ \beta_3^* = \frac{1}{(c^*)^2} [-\bar{y}_2 \Delta P + (c^*)^2 \Delta(\rho_2 z_2)], \\ \beta_4^* = \frac{1}{2(c^*)^2} [\Delta P + \underline{\rho} c^* \Delta u]. \end{cases}$$

Using the above formulas for $(\beta_k^*)_{k=1,\dots,4}$ allows to compute $\mathbf{R}(\mathbf{V}_L, \mathbf{V}_R)$ without computing M^* nor $(c_\alpha^*)^2$, $\alpha = 1, 2$. The sole value of $(c^*)^2$ is needed. Within the framework of stiffened gas EOS we chose

$$(c^*)^2 = \bar{y}_1 a_1 + \bar{y}_2 a_2.$$

The numerical scheme related to the convective part before the projection on equilibrium manifolds finally reads

$$\mathbf{W}_i^{n+1/2} = \mathbf{W}_i^n - \frac{\Delta t}{\Delta x} \left(\mathbf{G}_{i+1/2}^n - \mathbf{G}_{i-1/2}^n \right),$$

where the numerical flux $\mathbf{G}_{i+1/2}^n$ is given by

$$\mathbf{G}_{i+1/2} = \frac{1}{2} \begin{bmatrix} \rho_1 z_1 \\ \rho_2 z_2 \\ \rho u^2 + P \end{bmatrix}_{i+1} + \frac{1}{2} \begin{bmatrix} \rho_1 z_1 \\ \rho_2 z_2 \\ \rho u^2 + P \end{bmatrix}_i - \frac{1}{2} \mathbf{R}(\mathbf{V}_{i+1}, \mathbf{V}_i).$$

The color function z is advected using the following upwind scheme

$$z_i^{n+1/2} = z_i^n - \frac{\Delta t}{2\Delta x} \left[(\bar{u}_i^n - |\bar{u}_i^n|)(z_{i+1}^n - z_i^n) + (\bar{u}_i^n + |\bar{u}_i^n|)(z_i^n - z_{i-1}^n) \right].$$

Remark 8. The Roe-type solver described in this section can capture solutions that violate the entropy condition, e.g. when the solution comes across a sonic point. In order to remedy this flaw, we used the classical entropy fix introduced in [13] that consists in substituting $Q(\Lambda_j^, v)$ for $|\Lambda_j^*|$ in formula (32), where $v \in \mathbb{R}$ is a small parameter and*

$$Q(\Lambda_j^*, v) = \begin{cases} |\Lambda_j^*|, & \text{if } |\Lambda_j^*| > v, \\ \frac{1}{2} \left((\Lambda_j^*)^2 / v + v \right), & \text{if } |\Lambda_j^*| \leq v. \end{cases}$$

Let us underline that for the numerical tests we performed the above fix did not seem mandatory as it did not appear to carry a great influence with the numerical solution.

4.2 Relaxation Towards the M-Equilibrium (M-scheme)

For the M-equilibrium system, we suppose the parameter λ to be finite but very large. We formally set $\kappa = +\infty$ which imposes that the equilibrium value is retrieved by solving equation (19). With the stiffened gas assumption, we are able to give an explicit expression for z^* , namely

$$\begin{cases} z^* = \frac{\beta}{1 + \beta}, \\ \beta = \frac{-\left(a_2 m_2 - a_1 m_1 - P_2^\infty + P_1^\infty\right) + \sqrt{\left(a_2 m_2 - a_1 m_1 - P_2^\infty + P_1^\infty\right)^2 + 4a_1 a_2 m_1 m_2}}{2a_2 m_2}. \end{cases} \quad (33)$$

Remark 9. We emphasize once more that projection onto the M-equilibrium may be irrelevant when $m_1 m_2 = 0$, depending on the EOS used for the fluid 1 and the fluid 2. The relation (33) gives a good insight into this ambiguity. If one considers two EOS such that $P_2^\infty \neq P_1^\infty$ then for $m_1 = 0$ we have $\beta \neq 0$ which implies that $z^* \neq 0$. On the contrary, if one considers $P_2^\infty = P_1^\infty = 0$, then $\lim_{m_1 \rightarrow 0} \beta = 0$ and $\lim_{m_2 \rightarrow 0} \beta = 0$.

Using a splitting operator, we integrate over $[0, \Delta t]$ the following ODE system

$$\partial_t m_1 = \lambda \left[g_2(\rho_2) - g_1(\rho_1) \right], \quad \partial_t \rho = 0, \quad \partial_t(\rho u) = 0, \quad (34)$$

with initial condition $(\mathbf{W}, z)(0) = (\mathbf{W}, z)_i^{n+1/2}$.

For stability and maximum principle purpose, instead of a direct numerical integration of system (34), we seek for an approximate ODE system that allows explicit integration. In order to do so we scale parameter λ by setting $\lambda = m_1 m_2 \tilde{\lambda}$, where $\tilde{\lambda}$ is a supposed large constant parameter. Then, we also freeze the $(g_2 - g_1)$ term in its value $(g_2 - g_1)^{n+1/2}$ evaluated at $(\mathbf{W}, z)^{n+1/2}$. We obtain the simplified ODE system

$$\partial_t(m_1) = \tilde{\lambda} m_1 (\rho_i^{n+1/2} - m_1) (g_2 - g_1)_i^{n+1/2}, \quad \partial_t \rho = 0, \quad \partial_t(\rho u) = 0, \quad (35)$$

which can be solved explicitly

$$m_1(t) = \frac{\rho_i^{n+1/2}}{\left[\rho_i^{n+1/2} / (m_1)_i^{n+1/2} - 1 \right] \exp \left[-\tilde{\lambda} t \rho_i^{n+1/2} (g_2 - g_1)_i^{n+1/2} \right] + 1}, \quad (36)$$

and

$$\rho(t) = \rho_i^{n+1/2}, \quad u(t) = u_i^{n+1/2}.$$

Let us notice that the above relation ensures $m_1(t) \in [0, \rho(t)]$ for all $t > 0$. We now complete the source integration step by setting

$$\rho_i^{n+1} = \rho_i^{n+1/2}, \quad u_i^{n+1} = u_i^{n+1/2}, \quad (m_1)_i^{n+1} = m_1(\Delta t), \quad (m_2)_i^{n+1} = \rho_i^{n+1} - (m_1)_i^{n+1}.$$

Finally, we update z by remapping z onto the M-equilibrium states by using expression (33) with \mathbf{W}^{n+1} .

4.3 Relaxation Towards the MT-equilibrium (MT-scheme)

We now suppose the existence of densities $\rho_1^* < \rho_2^*$ solution of $P_1 = P_2$ and $g_1 = g_2$ known either explicitly in the case of perfect gases (see remark 4), either by solving (23) with an iterative algorithm for the case of stiffened gas. The intermediary solution $(\mathbf{W}^{n+1/2}, z^{n+1/2})$ obtained after the convective step (28) is projected onto the MT-equilibrium states using relation (24). This leads to

$$z_i^{n+1} = \begin{cases} 1 & \text{if } \rho_i^{n+1/2} < \rho_1^*, \\ \frac{\rho_i^{n+1/2} - \rho_2^*}{\rho_1^* - \rho_2^*} & \text{if } \rho_1^* < \rho_i^{n+1/2} < \rho_2^*, \\ 0 & \text{if } \rho_2^* < \rho_i^{n+1/2}, \end{cases}$$

for z_i^{n+1} ,

$$(m_1, m_2)_i^{n+1} = \begin{cases} (\rho_i^{n+1/2}, 0) & \text{if } \rho_i^{n+1/2} < \rho_1^*, \\ (\rho_1^* z_i^{n+1}, \rho_2^* (1 - z_i^{n+1})) & \text{if } \rho_1^* < \rho_i^{n+1/2} < \rho_2^*, \\ (0, \rho_i^{n+1/2}) & \text{if } \rho_2^* < \rho_i^{n+1/2}, \end{cases}$$

for partial densities of both phases and $\rho_i^{n+1} = \rho_i^{n+1/2}$, $u_i^{n+1} = u_i^{n+1/2}$.

5 Numerical Results

5.1 Pure Interface Advection

We consider a one dimensional advection problem: a 1 m long domain contains liquid and vapor initially separated by an interface located at $x = 0.5$ m. Both fluids $\alpha = 1, 2$ are governed by a stiffened EOS (see relation 22) where the parameters $(a_\alpha, b_\alpha, P_\alpha^\infty)_{\alpha=1,2}$, of the fluids are given in table 1. Velocities of both fluids are fixed at $u = 100 \text{ m.s}^{-1}$ and densities are chosen on each side of the interface such that the pressure is constant in the whole domain, namely $\rho = \rho_1^* = 1.0 \text{ kg.m}^{-3}$ on the left (fluid 1) and $\rho = \rho_2^* = 2.0 \text{ kg.m}^{-3}$ on the right (fluid 2).

	fluid 1 (left)	fluid 2 (right)
P^∞ (Pa)	0	0.5
a (Pa.kg ⁻¹ .m ³)	1.5	1.0
b (J)	ln(2)	0

Table 1: Fluids parameters for the pure advection test.

Boundary conditions are constant states on both side of the domain which is discretized over 100 cells. Figure 6 displays the solution obtained with the MT-scheme

(dots) and the solution obtained with the Roe scheme applied to the system (15) without source terms (solid lines).

Although this test is a simple Riemann problem which does not involve phase change but purely kinetic effects, we emphasize the fact that the MT-equilibrium system we deal with does not match the classical hyperbolic well-posedness criteria. However, we can check that the MT-scheme seems to capture the same advected profile as the Roe scheme applied to (15) without source terms. Indeed, we obtain the same propagation speed without any pressure nor velocity perturbations.

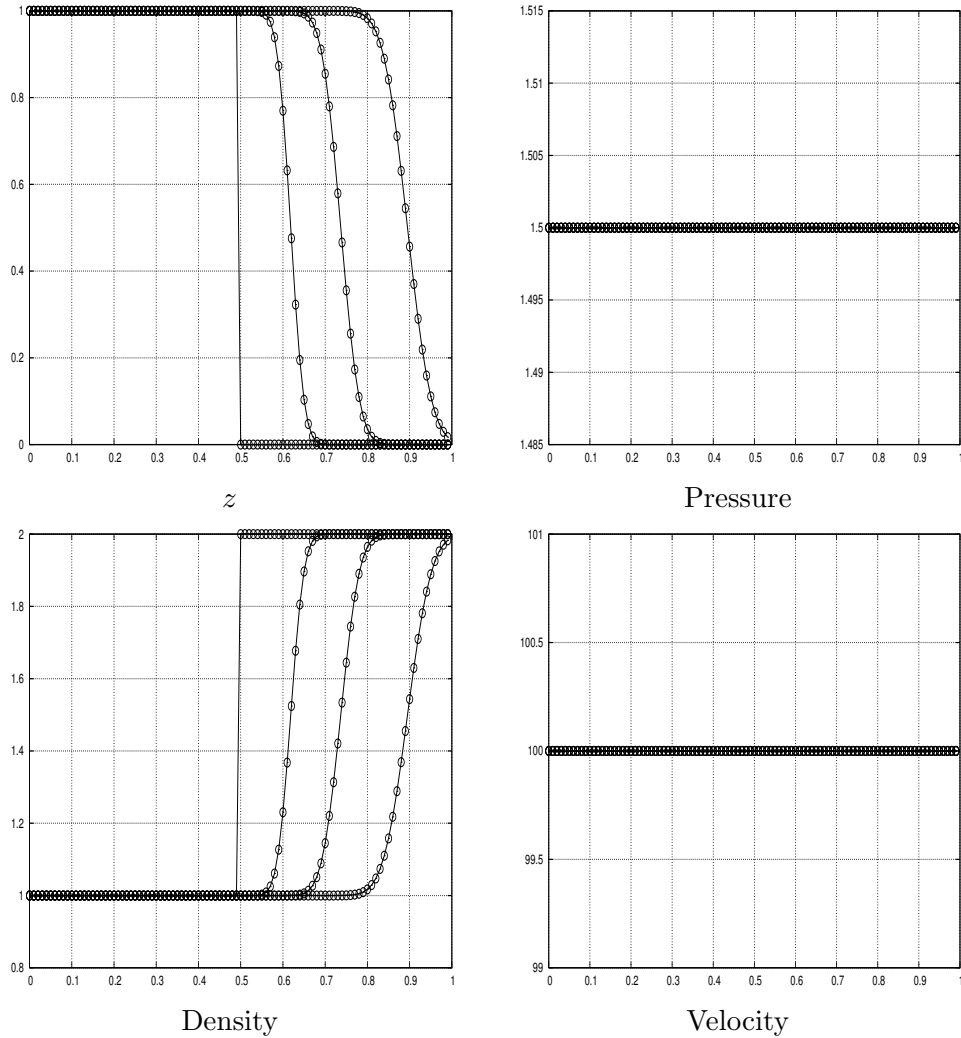


Figure 6: Time evolution of the MT-equilibrium solution computed with MT-scheme (dots) and the solution of the pure convective part of the system (15) computed with a Roe scheme (solid lines); t varies from $t = 0$ s to $t = 4$ ms.

5.2 A One dimensional Isothermal Phase Change Test

We now turn to the case of a one dimensional phase change test. As previously, we consider a 1 m long domain containing liquid and vapor initially separated by an interface located at $x = 0.5$ m. We suppose that both phases are perfect gas (characteristics parameters are given in table 2). In the whole domain, the fluid is supposed to be initially at rest at constant temperature $T = 100$ K, and the densities are once again chosen so that pressure is constant: $\rho = \rho_1^* \simeq 0.605921124862 \times 10^{-3}$ kg.m⁻³ on the left and $\rho = \rho_2^* \simeq 3.32172681063 \times 10^{-3}$ kg.m⁻³ on the right.

We now suppose that the left boundary is a piston which moves towards left at constant speed $u_p = -100$ m.s⁻¹ while the right boundary condition is a reflecting wall. The piston boundary condition is implemented using fictitious cells where the velocity is set to $u = u_p$. This piston motion will generate an acoustic wave travelling from left to right that will reach the interface location, perturbing its thermodynamical equilibrium and triggering source terms. A phase change process occurs.

	left (vapor)	right (liquid)
c_v (J.kg ⁻¹ .K ⁻¹)	1 816	1 040
$\gamma = c_p/c_v$	2.35	1.43
T (K)	100	100

Table 2: Fluids parameters for the piston test.

5.2.1 Mesh Convergence

Figures 7 and 8 represent profiles comparison for z , density, pressure and velocity obtained with MT-equilibrium scheme for different meshes. Symbols ∇ and \times represent respectively solutions obtained with a domain discretize over 100 and 1000 cells while solid lines represent solutions obtained with a domain discretized over 5000 cells. This allows us to check the convergence behaviour of the solution obtained with the MT-equilibrium scheme when the space step goes to zero. We note that no instability occurs except for the pressure in front of the interface.

5.2.2 M-Equilibrium Solution versus MT-equilibrium Solution

We now turn towards the convergence of the solution obtained with the M-equilibrium scheme to the solution obtained with the MT-equilibrium scheme when the $\tilde{\lambda}$ parameter goes to $+\infty$. Figures 9 and 10 represent z , density, pressure and velocity profiles obtained with both schemes at time $t = 15$ ms for the piston test case; $\tilde{\lambda}$ varies from 10 to 10^6 and the domain is discretized over 300 cells. Solid lines represent solution obtained with the MT-equilibrium schemes while symbols represent solution obtained with the M-equilibrium scheme. This allows us to check the convergence of the M-equilibrium solution to the MT-equilibrium solution when parameter $\tilde{\lambda}$ goes

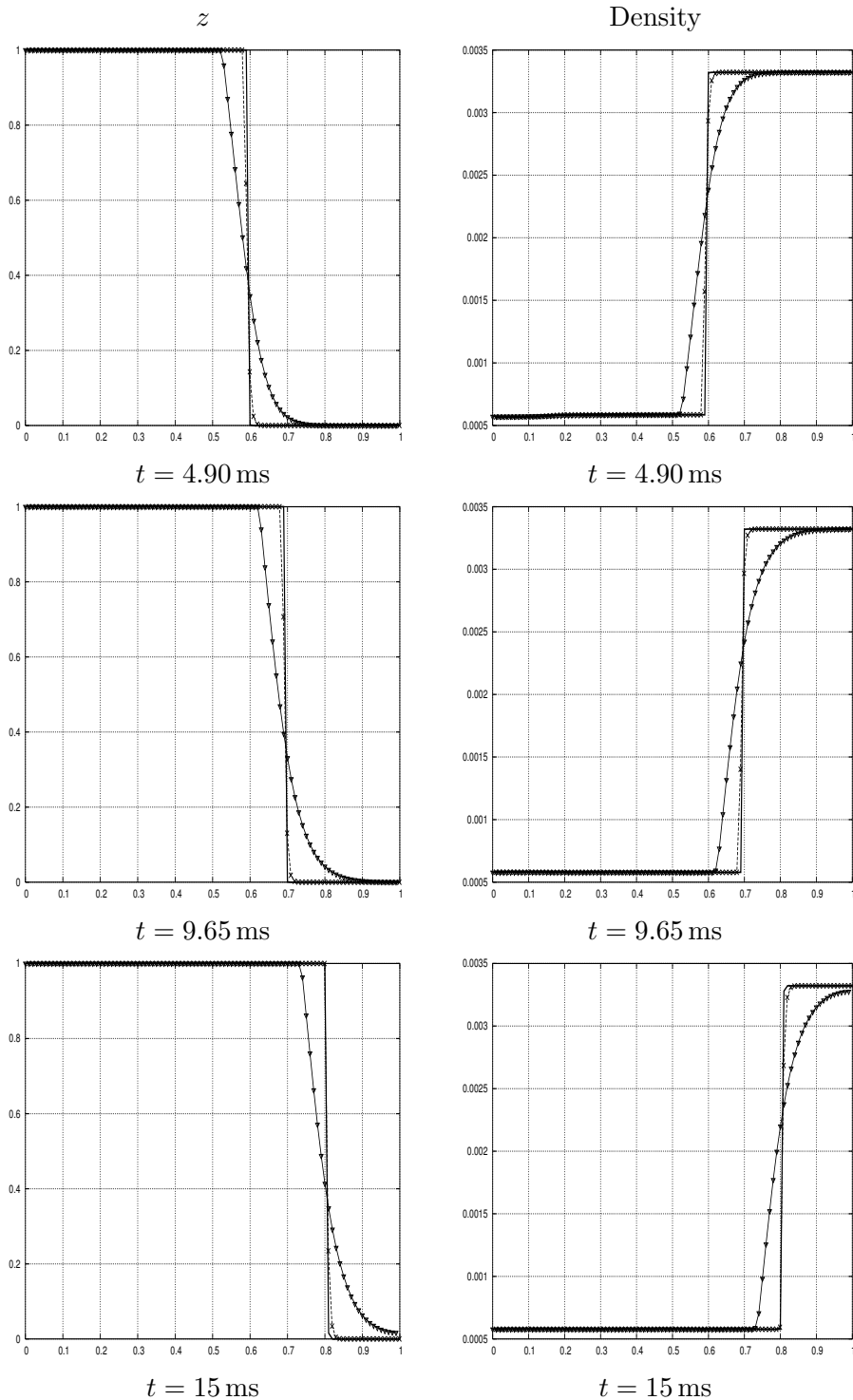


Figure 7: z and density profiles comparison between solutions for different mesh sizes obtained with the MT-equilibrium scheme; symbols ∇ and \times represent respectively solutions obtained with a domain discretize over 100 and 1000 cells while solid lines represent solutions obtained with a domain discretized over 5000 cells.

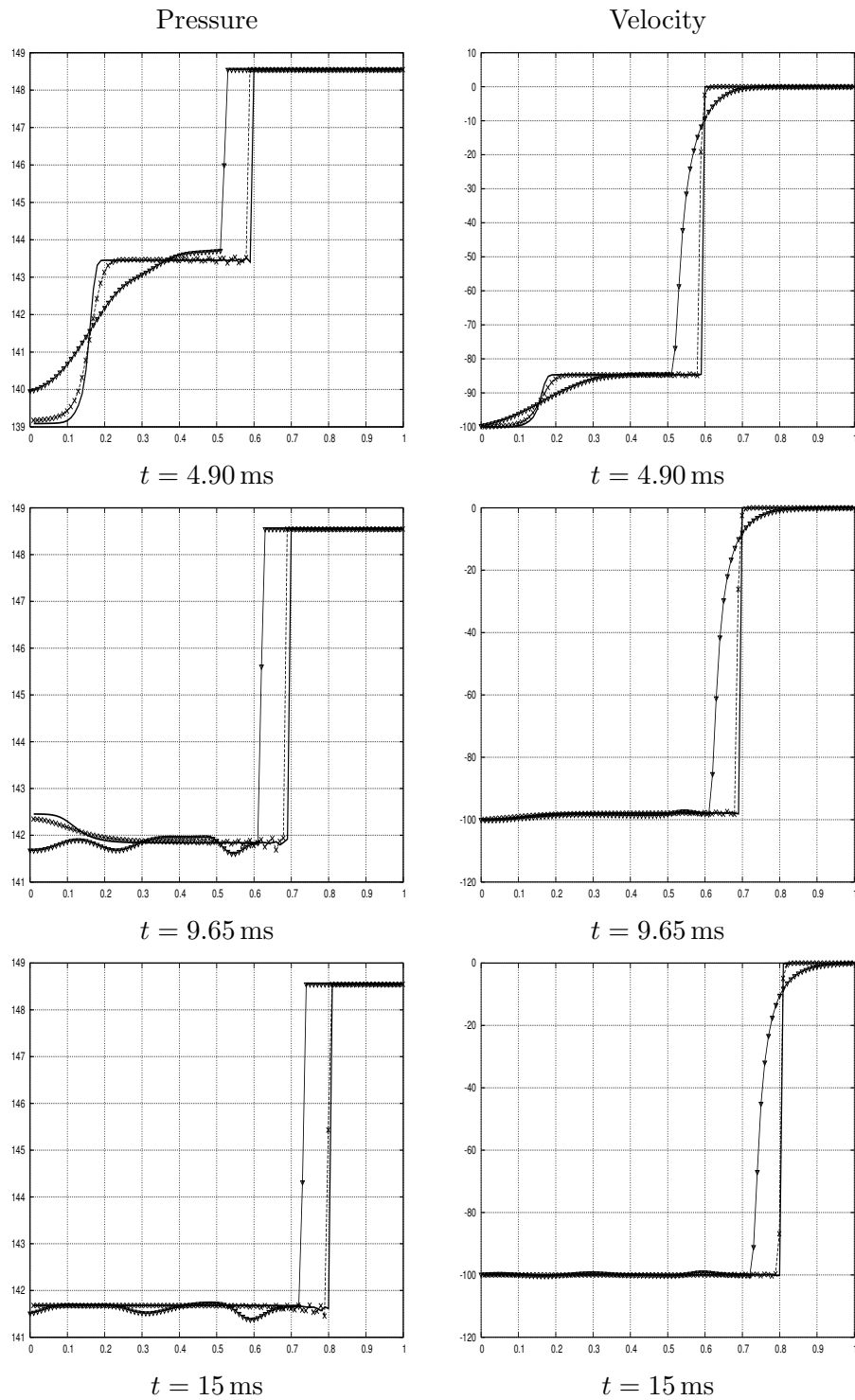


Figure 8: Pressure and velocity profiles comparison between solutions for different mesh sizes obtained with the MT-equilibrium; symbols ∇ and \times represent respectively solutions obtained with a domain discretize over 100 and 1000 cells while solid lines represent solutions obtained with a domain discretized over 5000 cells.

to $+\infty$.

For this test, we experienced stability issues with the M-equilibrium due to the integration step based on relation (36) when $\tilde{\lambda} > \tilde{\lambda}_{\max} = 10^3$ (this value is not optimal). We adopted a straightforward remedy that consists in splitting the single integration step using $\tilde{\lambda}$ in $r_{\max} \in \mathbb{N}$ integration steps using $\tilde{\lambda}_{\max}$, where $r_{\max} = \lceil \tilde{\lambda}/\tilde{\lambda}_{\min} \rceil + 1$. Let us briefly describe this procedure: we define for $r \in \mathbb{N}$, $1 \leq r \leq r_{\max}$

$$\left\{ \begin{array}{l} (m_1)_i^{n+1/2,r+1} = \frac{\rho_i^{n+1/2,r}}{\left[\frac{\rho_i^{n+1/2,r}}{(m_1)_i^{n+1/2,r}} - 1 \right] \exp \left[-\tilde{\lambda}_{\max} \rho_i^{n+1/2,r} (g_2 - g_1)_i^{n+1/2,r} \Delta t \right] + 1}, \\ (m_2)_i^{n+1/2,r+1} = \rho_i^{n+1/2,r} - (m_1)_i^{n+1/2,r+1}, \\ \rho_i^{n+1/2,r+1} = \rho_i^{n+1/2,r}, \\ u_i^{n+1/2,r+1} = u_i^{n+1/2,r}, \\ z_i^{n+1/2,r+1} \text{ is updated by mapping } (m_1, m_2)_i^{n+1/2,r+1} \text{ onto the M-equilibrium,} \end{array} \right.$$

with

$$(m_1, m_2, u, z)^{n+1/2,r=0} = (m_1, m_2, u, z)^{n+1/2}.$$

And finally we set

$$(m_1, m_2, u, z)^{n+1} = (m_1, m_2, u, z)^{n+1/2,r_{\max}}.$$

We emphasize that the above lines are just a simple and rough cure for the stability issues. More efficient solutions in term of CPU cost are still to be considered.

We now take the MT-equilibrium solution as the reference solution marked \mathbf{V}_h^{ref} and we note $\mathbf{V}_h^{\tilde{\lambda}}$ the solution obtained with the M-equilibrium scheme when $\tilde{\lambda}$ is large but finite. Figure 11 represents $\log(\tilde{\lambda}) \mapsto \log(\|a_h^{\tilde{\lambda}} - a_h^{ref}\|_{L^2})$ for some different a which indicates respectively z , density, pressure and velocity.

5.2.3 Time Convergence

We now study the convergence of the solution obtained with the M-scheme when the time step goes to zero. It is well known that integration of stiff source terms (when $\tilde{\lambda}$ is large) could produce wrong propagation speed for the interface (see [18] for instance). Actually, in some cases, the interface pulls forward some fixed number of cells. Then, when the time step decreases, the interface seems to go faster. This numerical artefact could appear when we do not project solution on the $\{P_1 = P_2\}$ variety. Figure 12 shows the solution obtained with the M-equilibrium scheme with two CFL conditions; solid lines show numerical solution obtained with the second CFL condition

$$\Delta t = \frac{1}{2} \frac{\Delta x}{\max_{i=1,4} |\Lambda_k|}, \quad (37)$$

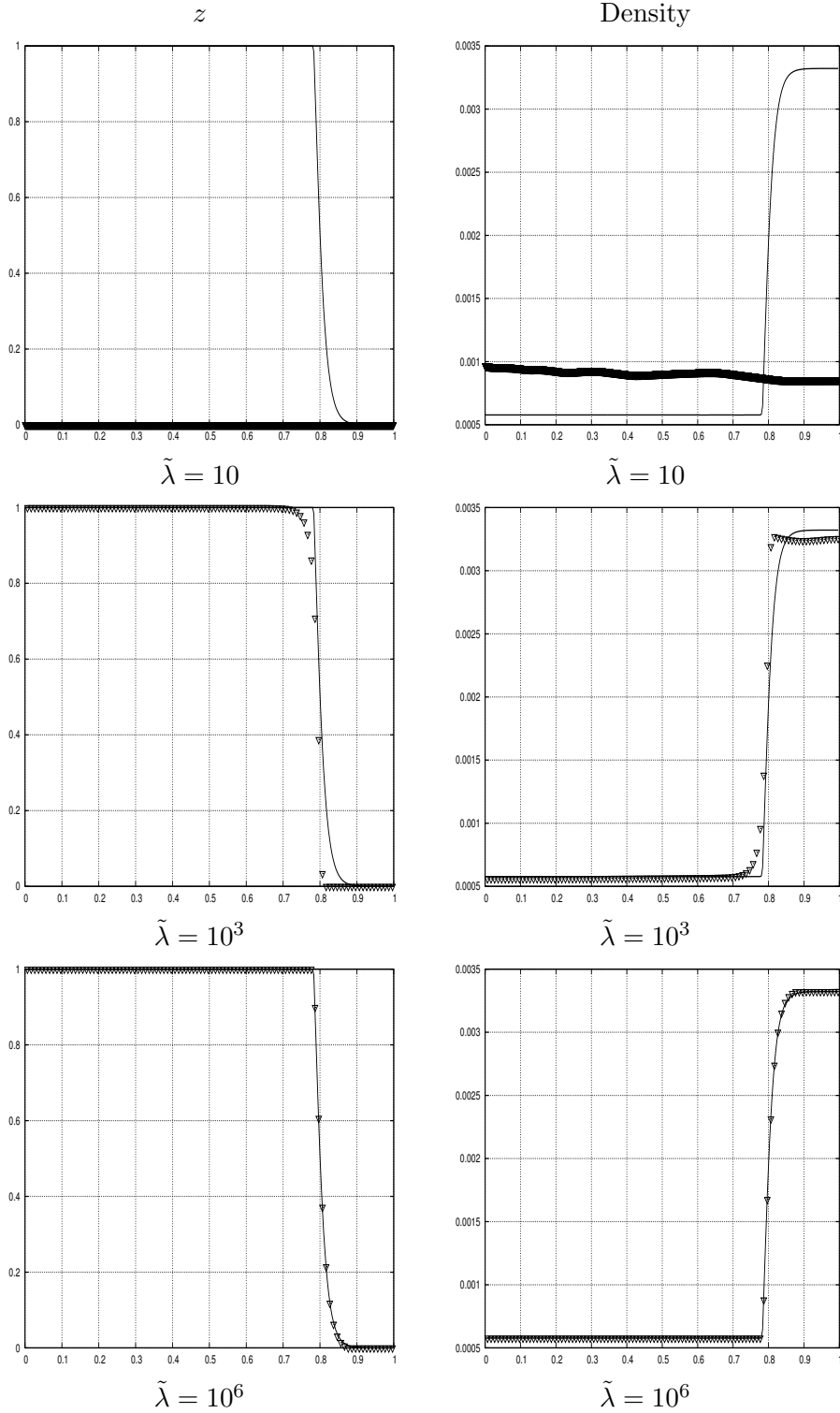


Figure 9: z and density profiles comparison between M-equilibrium solution and MT-equilibrium solution; $t = 15$ ms, $\tilde{\lambda}$ is ranged from 10 to 10^6 .

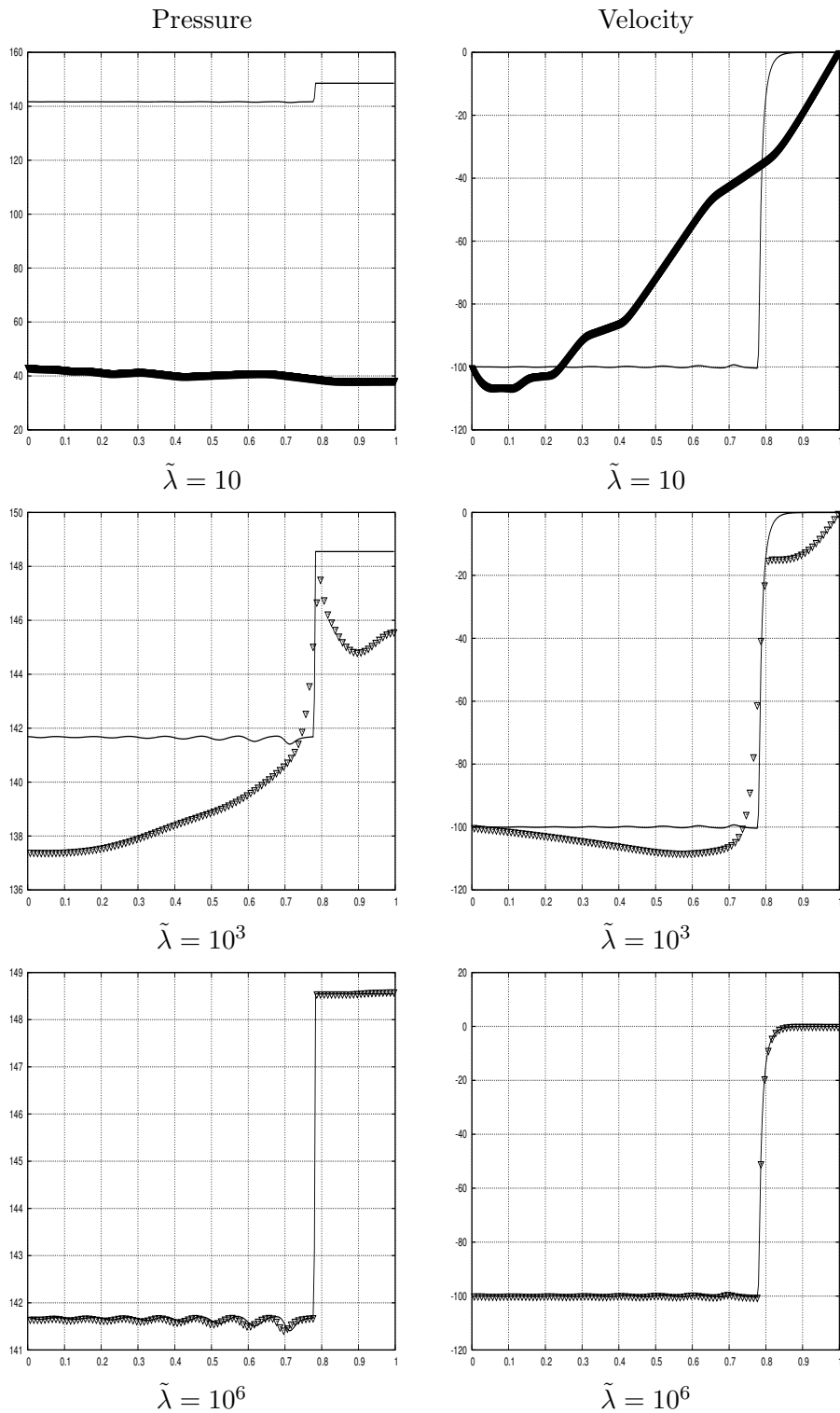


Figure 10: pressure and velocity profiles comparison between M-equilibrium solution and MT-equilibrium solution; $t = 15$ ms, $\tilde{\lambda}$ is ranged from 10 to 10^6 .

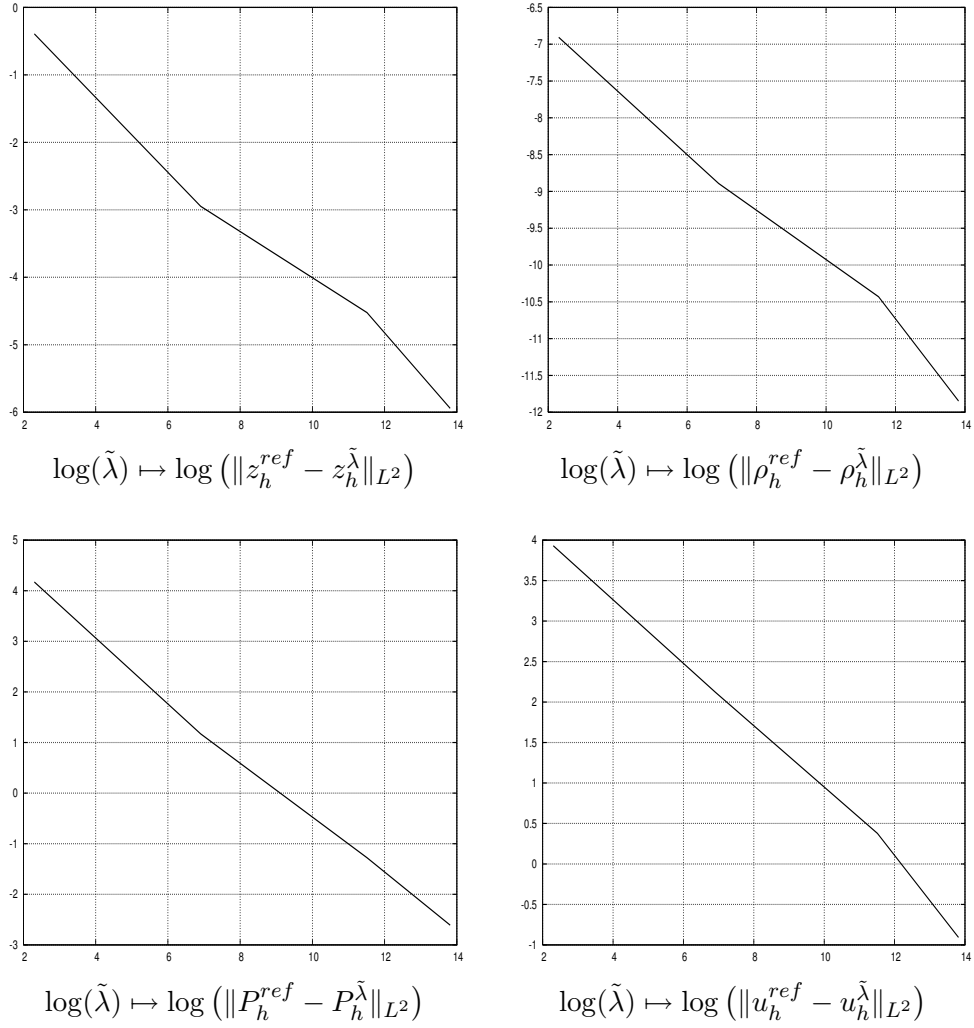


Figure 11: M-equilibrium solution convergence towards MT-equilibrium solution when $\tilde{\lambda}$ goes to $+\infty$; $\tilde{\lambda}$ is ranged from 10 to 10^6 .

while ∇ symbols show numerical solution obtained with the following CFL condition

$$\Delta t = \frac{1}{200} \frac{\Delta x}{\max_{i=1,4} |\Lambda_k|}. \quad (38)$$

The domain is discretized over 100 cells and $\tilde{\lambda}$ is fixed at 10^6 . This show us that the numerical solution, and consequently the velocity of the interface, does not depend on the time step.

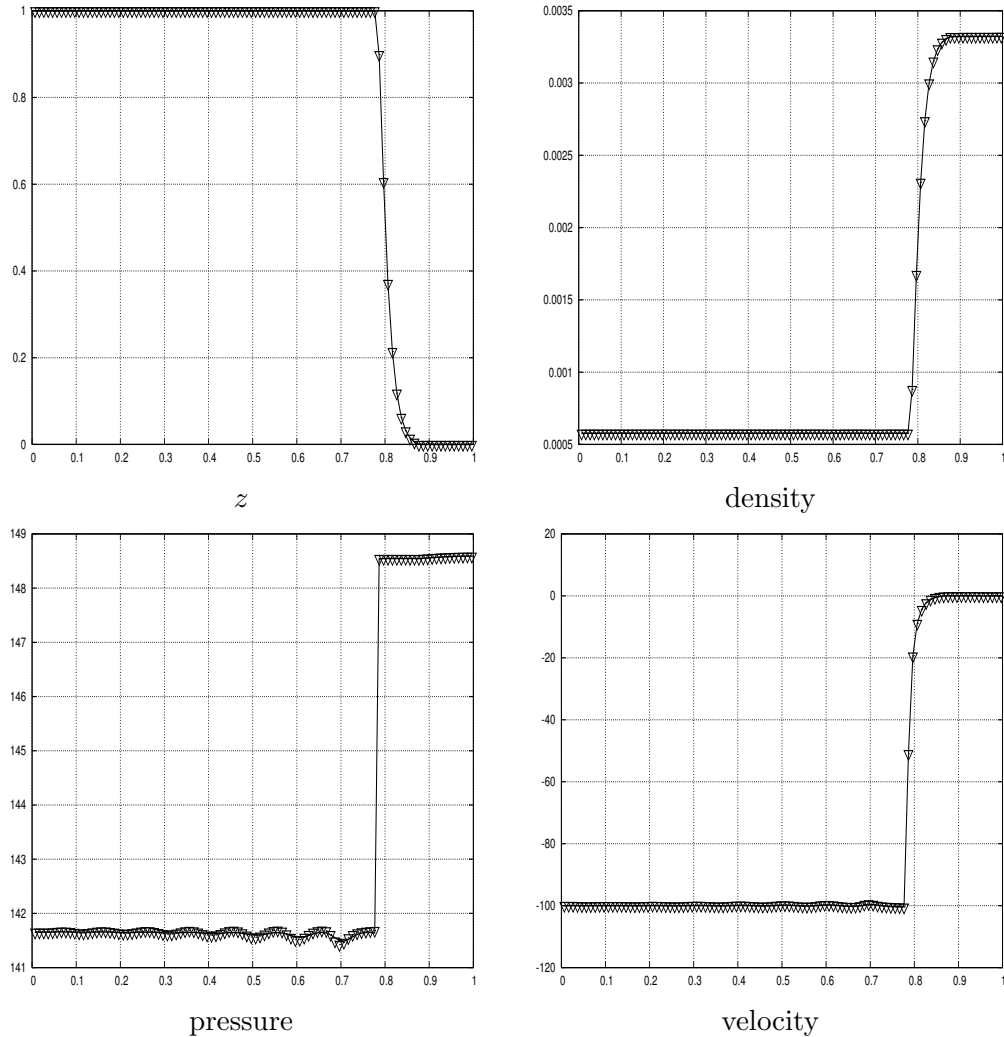


Figure 12: z , density, pressure and velocity profiles comparison for solutions obtained with the M-equilibrium scheme; the time step is given by CFL condition (37) (solid lines) and (38) (∇ symbols).

5.3 Compression of a Gas Bubble

We consider a 1 m long square domain discretized over 100×100 cells mesh. A vapor bubble is surrounded by liquid in the center of the domain. The radius is initially $r = 25$ cm. The EOS used are stiffened gas type whose coefficients are given in table 1. The temperature is fixed to $T = 600$ K and densities are given by $\rho_1^* \simeq 35.5 \text{ k.m}^{-3}$ for the vapor and $\rho_2^* \simeq 686.25 \text{ kg.m}^{-3}$ for the liquid.

We suppose the left boundary be a piston moves toward right at constant speed $u_p = 100 \text{ m.s}^{-1}$. The other boundary conditions are reflecting wall. Figure 13 shows the z profile obtained with the MT-scheme (on the left) and the z profile obtained with the homogeneous system (on the right) at various instants. We notice that with the MT-scheme, a phase change occurs and the vapor bubble liquefies while for the off-equilibrium system (15) without source terms, the bubble is just compressed.

5.4 Depression of Two Liquid Drops

We again consider a 1 m long square domain discretized over 100×100 cells where two drops of dodecan liquid are surrounded by dodecan vapor. Both equations of state are stiffened gas type whose coefficients are given in table 3. Temperature is fixed at 600 K and as previously, densities of liquid and vapor are chosen such that phases are at mechanic and thermodynamic equilibrium, namely $\rho_1^* = 12.08 \text{ kg.m}^{-3}$ for the vapor and $\rho_2^* = 458.62 \text{ kg.m}^{-3}$ for the liquid.

	liquid	vapor
c_v (J.kg ⁻¹ .K ⁻¹)	1077.7	1956.45
$\gamma = C_p/C_v$	2.35	1.025
P^∞ (Pa)	4.10^8	0
q (kJ.kg ⁻¹)	-755.269	-237.547
q' (kJ.kg ⁻¹ .K ⁻¹)	0	-24.485

Table 3: Fluid parameters for liquid and vapor dodecan.

On the left of the domain, a depression is simulated by imposing a constant velocity $u_p = -100 \text{ m.s}^{-1}$ in fictitious cells. Other boundary conditions are reflective walls. Figures 14, 15, 16 and 17 show respectively z , density, pressure and velocity in the x -direction profiles for time varying from $t = 2$ ms to $t = 32$ ms. This allows us to show the vaporization of liquid bubbles due to the depression.

6 Conclusion

We have presented in this paper a dynamical phase-change model for compressible flows. The physical model derivation has been detailed. We have proposed a numerical Finite-Volume based discretization approach which complies with the entropy balance of the model. This feature is important as uniqueness fails in the

general class of entropy solutions for the equilibrium MT-equilibrium system. In this way, while ill-posedness for this model is still an open issue, we can conjecture that the approximate solution obtained with our approach complies with the dissipative structures of the relaxed model.

The present modelling and numerical approach extend to the anisothermal framework with little efforts. It has been recently achieved in [5]. Even stronger connections with the seminal work of Jaouen [16] and Barberon & Helluy [3, 14], which are not yet clarified, are to be expected.

References

- [1] G. Allaire, S. Clerc, and S. Kokh. A five-equation model for the numerical simulation of interfaces in two-phase flows. *C. R. Acad. Sci. Paris, Série I*, t. 331:pp. 1017–1022, 2000.
- [2] G. Allaire, S. Clerc, and S. Kokh. A five-equation model for the simulation of interfaces between compressible fluids. *J. Comp. Phys.*, 181:pp. 577–616, 2002.
- [3] T. Barberon and Ph. Helluy. Finite volume simulation of cavitating flows. *Computers and Fluids*, 34(7):pp. 832—858, 2005.
- [4] A. Bedford. *Hamilton's principle in continuum mechanics*. Research Notes in Mathematics, 1985.
- [5] F. Caro. *Modélisation et simulation numérique des transitions de phase liquide-vapeur*. PhD thesis, Ecole Polytechnique, 2004.
- [6] F. Caro, F. Coquel, D. Jamet, and S. Kokh. DINMOD: A diffuse interface model for two-phase flows modelling. In S. Cordier, T. Goudon, M. Gutnic, and E. Sonnendrücker, editors, *Numerical methods for hyperbolic and kinetic problems, IRMA lecture in mathematics and theoretical physics (Proceedings of the CEMRACS 2003)*, 2005.
- [7] F. Caro, F. Coquel, D. Jamet, and S. Kokh. Phase change simulation for isothermal compressible two-phase flows. In *AIAA Comp. Fluid Dynamics*, number AIAA-2005-4697, 2005.
- [8] P. Casal and H. Gouin. A representation of liquid-vapor interfaces by using fluids of second gradient. *Annales de physique, Colloque num. 2*, 13, 1988.
- [9] G. Chanteperdrix, Ph. Villedieu, and J.P. Vila. A compressible model for separated two-phase flows computations. In *Proceedings os ASME Fluid Eng. Div. Summer Meeting 2002*, 2002. Paper 3114.
- [10] J.M. Delhaye, M. Giot, and M.L. Riethmuller. *Thermohydraulics of Two-Phase Systems for Industrial Design and Nuclear Engineering*. Hemisphere Publishing Corporation, 1981.

-
- [11] S. Gavriluk and H. Gouin. A new form of governing equations of fluids arising from Hamilton's principle. *International Journal of Engineering Science*, 37, 1999.
- [12] S. Gavriluk and R. Saurel. Mathematical and numerical modeling of two-phase compressible flows with micro-inertia. *J. Comp. Phys.*, 175:326–360, 2002.
- [13] A. Harten and J.M. Hyman. Self adjusting grid methods for one-dimensional hyperbolic conservation laws. *J. Comp. Phys.*, 50:pp. 235–269, 1983.
- [14] Ph. Helluy. Simulation numérique des écoulements multiphasiques : de la théorie aux applications.(thèse d'habilitation). Technical report, 2005.
- [15] D. Jamet, O. Lebaigue, N. Coutris, and J.M. Delhayé. The second gradient method for the direct numerical simulation of liquid-vapor flows with phase change. *J. Comp. Phys.*, 169:624–651, 2001.
- [16] S. Jaouen. *Etude mathématique et numérique de stabilité pour des modèles hydrodynamiques avec transition de phase*. PhD thesis, Univ. Paris 6, 2001.
- [17] F. Lagoutière. *Modélisation mathématique et résolution numérique de problèmes de fluides à plusieurs constituants*. PhD thesis, Univ. Paris 6, 2002.
- [18] R. J. LeVeque and H. C. Yee. A study of numerical methods for hyperbolic conservation laws with stiff source terms. *J. Comp. Phys.*, 86:187–210, 1990.
- [19] J. Massoni, R. Saurel, B. Nkonga, and R. Abgrall. Proposition de méthodes et modèles eulériens pour les problèmes à interfaces entre fluides compressibles en présence de transfert de chaleur: Some models and eulerian methods for interface problems between compressible fluids with heat transfer. *Int. J. of Heat and Mass Transfer*, 45(6):pp. 1287–1307, 2002.
- [20] O. Le Metayer. *Modélisation et résolution de la propagation de fronts perméables: application aux fronts d'évaporation et de détonation*. PhD thesis, Université de Provence (Aix-Marseille 1), 2003.
- [21] P.L. Roe. Approximate Riemann solvers, parameter vectors and difference schemes. *J. Comp. Phys.*, 43:pp. 357–372, 1981.
- [22] R. Salmon. Hamiltonian fluid mechanics. *Ann. Rev. Fluid Mech.*, (20):pp. 225–256, 1988.
- [23] L. Truskinovsky. Kinks versus shocks. In R. Fosdick and al., editors, *Shock induced transitions and phase structures in general media*. Springer Verlag, Berlin, 1991.

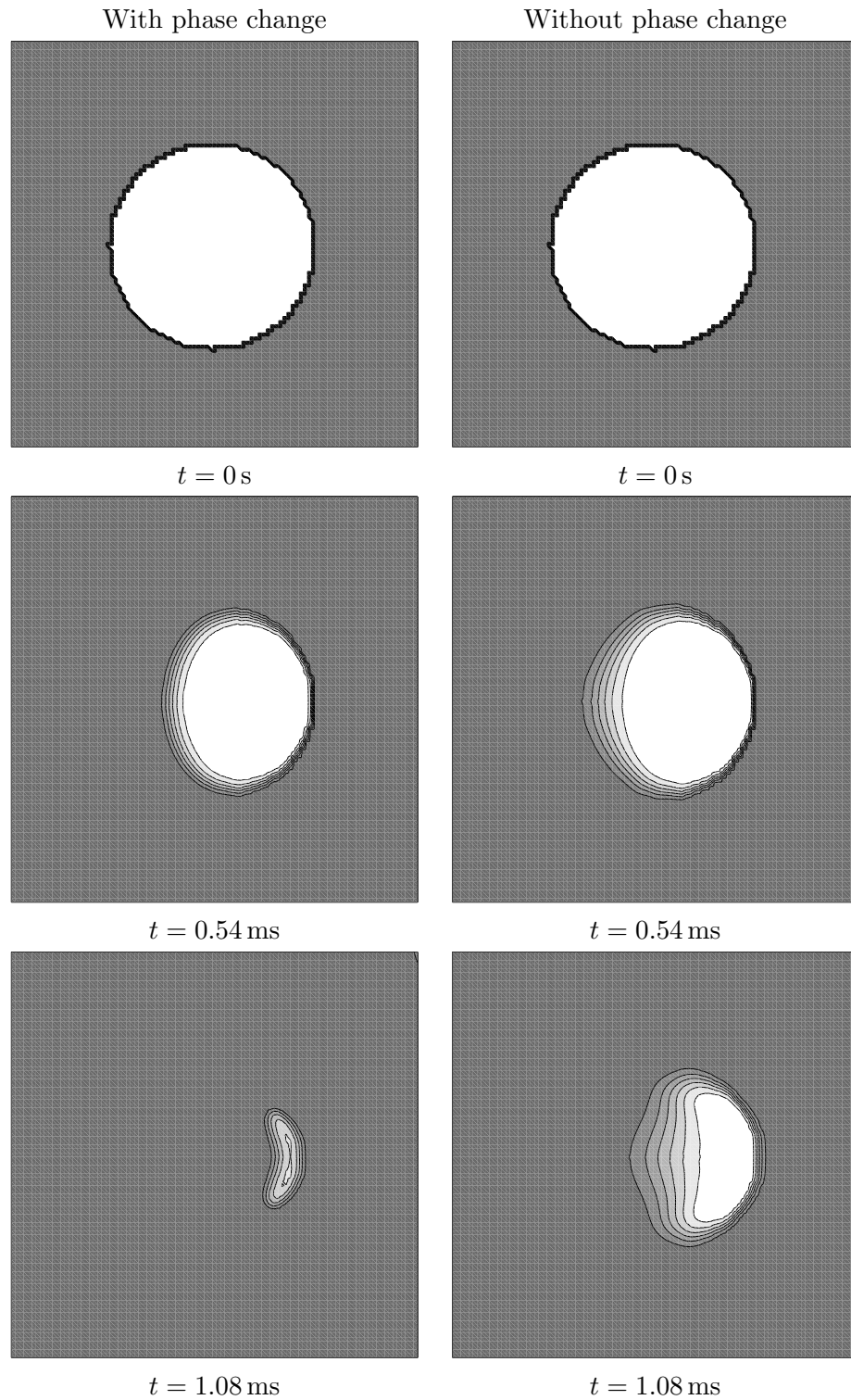


Figure 13: z profile obtained with the MT-scheme on the bottom and z profile obtained with the homogeneous system on the top; t varies from $t = 0\text{ s}$ to $t = 1.08\text{ ms}$.

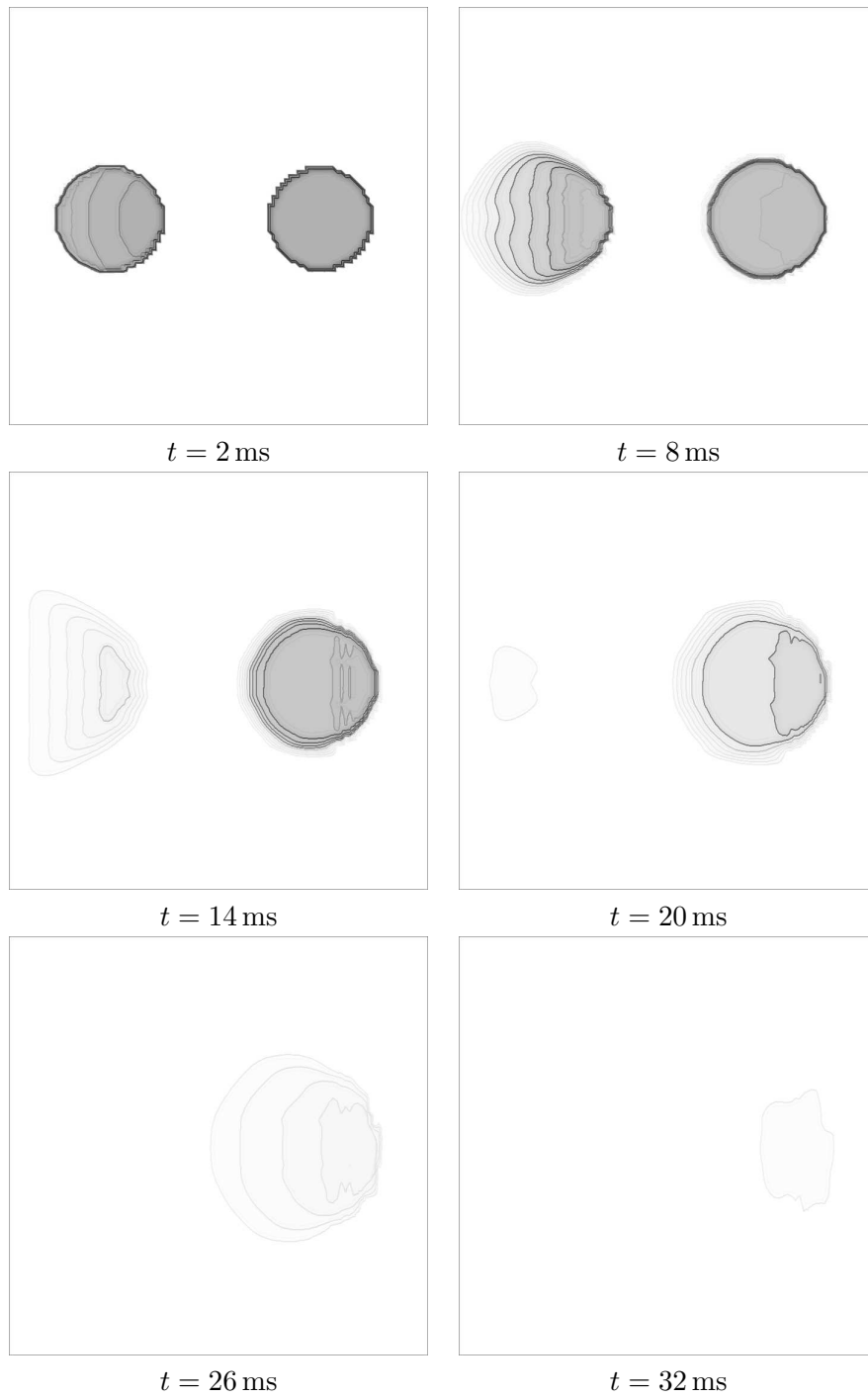


Figure 14: z profile obtained with the MT-equilibrium scheme; t varies from 2 ms to 32 ms.

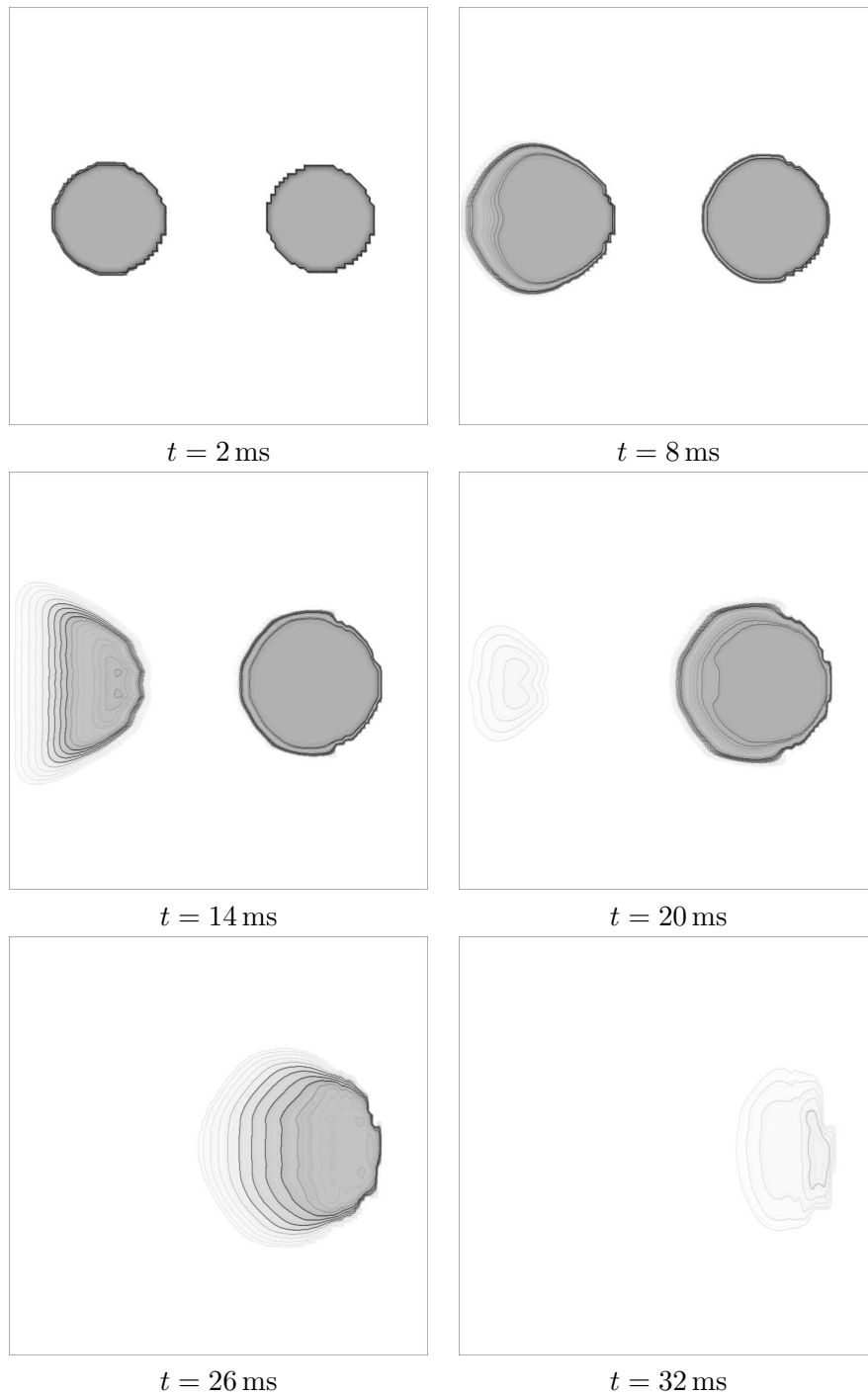


Figure 15: Density profile obtained with the MT-equilibrium scheme; t varies from 2 ms to 32 ms.

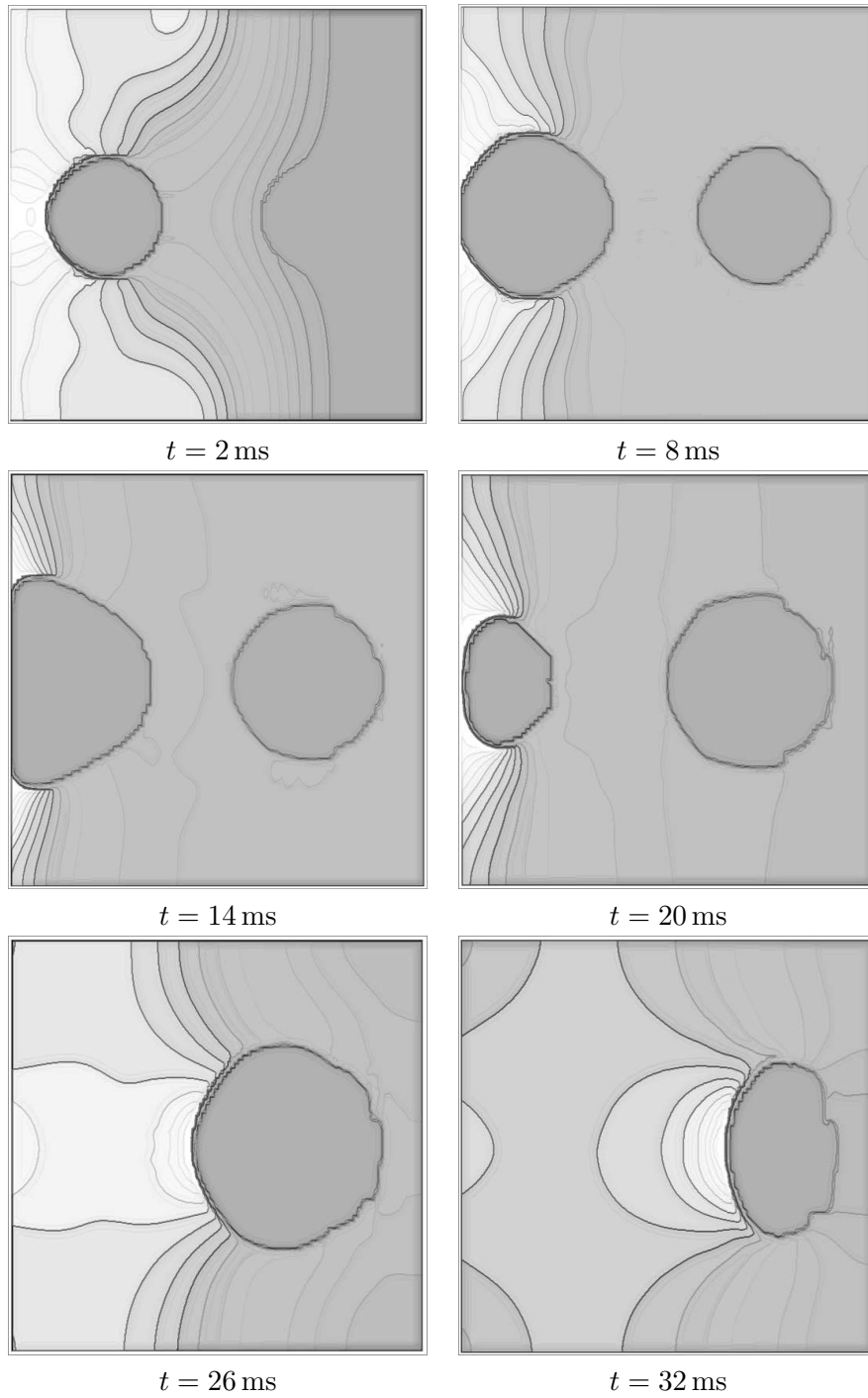


Figure 16: Pressure profile obtained with the MT-equilibrium scheme; t varies from 2 ms to 32 ms.

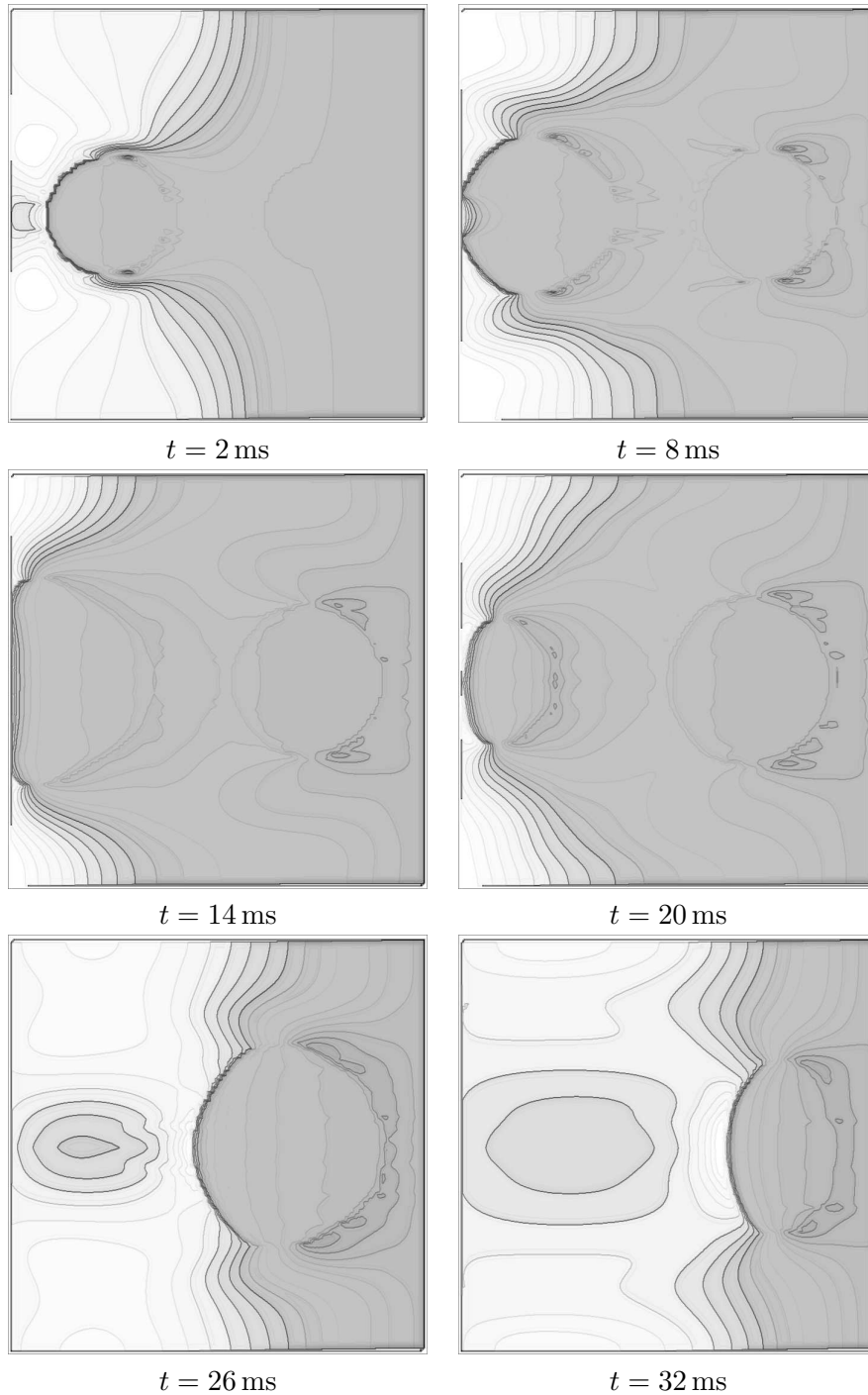


Figure 17: Velocity in the x -direction profile obtained with the MT-equilibrium scheme; t varies from 2 ms to 32 ms.